COMITATO NAZIONALE PER L'ENERGIA NUCLEARE
Laboratori Nazionali di Frascati

LNF-75/27(R)
22 Maggio 1975

G. Bellettini: LARGE MOMENTUM TRANSFER PHENOMENA

Servizio Documentazione
dei Laboratori Nazionali di Frascati del CNEN
Casella Postale 70 - Frascati (Roma)

Laboratori Nazionali di Frascati del CNEN
Servizio Documentazione

LNF-75/27(R)
22 Maggio 1975

G. Bellettini

Istituto Nazionale di Fisica Nucleare, Laboratori Nazionali di Frascati
and
Istituto di Fisica dell'Università di Pisa

LARGE MOMENTUM TRANSFER PHENOMENA(x)

An experimental review is given on single hadron and lepton production at large momentum transfer in hadron-hadron collisions and on associated particle correlations.

(x) - Lecture delivered at the "1975 Yerevan School on High Energy Physics", April 1975, Yerevan (USSR).

INTRODUCTION. -

One of the most interesting phenomena which was put in evidence by experiments at the ISR and Fermi Lab. concerned the production of particles at large momentum transfer ($P_\perp \gtrsim 1$ GeV/c), which was found to be much more abundant than expected from the observed production at small $P_\perp$. In addition particles produced in association with large $P_\perp$ secondaries were found to exhibit a number of peculiar features, which are closely related to the underlying production mechanism. A number of good and rather complete theoretical and experimental summaries on this subject exist already[1]. In this paper, an experimental review of the most relevant data in this field as of spring of 1975 will be given.

This subject is naturely splitted into three topics, that we shall discuss in three separate sections:

1) Inclusive single hadron production at large $P_\perp$. It will be shown that the pion data exhibit a surprisingly large cross section at large $P_\perp$, which grows with energy according to an approximate scaling law. The other particles show appreciable differences with respect to pions.

2) Particle correlations in large $P_\perp$ events. In these events, the secondaries are found to be strongly correlated to the large $P_\perp$ particle, in a way which is suggestive of a two-jet structure.

3) Inclusive direct lepton production at large $P_\perp$. The data show that the cross section for this process is qualitatively similar to that of hadron production but the observed rate is so high (about 10^{-4} of the pions) that it cannot easily be explained as due to leptonic decays of short lived resonances. This result suggests the existence of some new particles or some new mechanism which couples leptons to hadrons.

1. - INCLUSIVE SINGLE HADRON PRODUCTION AT LARGE $P_\perp$. -

A number of experiments at the ISR and Fermi Lab. have measured single hadron production at large $P_\perp$ [2]. Several important features have been observed:

a) The invariant cross sections show a slow fall-off at large $P_\perp$ compared with a fast exponential fall-off at small $P_\perp$;

b) The invariant cross-sections rise with increasing s at large $P_\perp$;

c) Heavy particles are produced relatively more copiously at large $P_\perp$ than at small $P_\perp$.

Relevant data on a) was first reported by the CERN-Columbia-Rockfeller (CCR) Collaboration studying at the ISR the inclusive π^o spectrum at $\theta_{CM} \approx 90^o$ [3]. Fig. 1 shows the experimental layout of the CCR experiment for detecting photons from π^o decays. The signature and the energy of the π^o are given by the double arrays of lead glass Cerenkov counters. The scintillation counters provide part of the beam-beam trigger by signalling those interactions in which at least one charged track was produced in association with the π^o.

The invariant cross section for inclusive π^o production at large $P_\perp$ and at $\theta_{cm} = 90^o$ for five different ISR momenta P_{ISR} ($2P_{ISR} = \sqrt{s}$) are shown in Fig. 2. The dashed line is the extrapolation of the exponential fall-off at low $P_\perp$. The data can be parametrized as

$$E\frac{d\sigma}{d^3p} = A P_\perp^{-N} e^{-Bx_\perp}, \qquad x_\perp = \frac{2P_\perp}{\sqrt{s}}, \qquad A = (1.54 \pm 0.10)\,10^{-26}\ \text{cm}^2\,\text{GeV}^{N-2}\ \text{sr}^{-1} \tag{1}$$

$$B = 13.05 \pm 0.25, \qquad N = 8.24 \pm 0.05$$

Therefore the CCR data are found to scale with energy as shown in Fig. 3. It should be observed that if the production was due to point like interactions like in deep inelastic electron scattering, one would expect $N = 4$ [4].

In the above mentioned π^o experiment, photon pairs coming from η decays were not distinguished from those coming from π^o decays. The production of high P η-mesons has been recently reported by the CERN-Columbia-Rockfeller-Saclay group[5]. The results, at $\sqrt{s} = 52.7$ GeV, show a clear η signal from an invariant mass plot of the two photons. The η signal amounts to approximately 46% of the π^o signal. The $P_\perp$ dependence of the η cross section is also similar to the π^o as shown in Fig. 4.

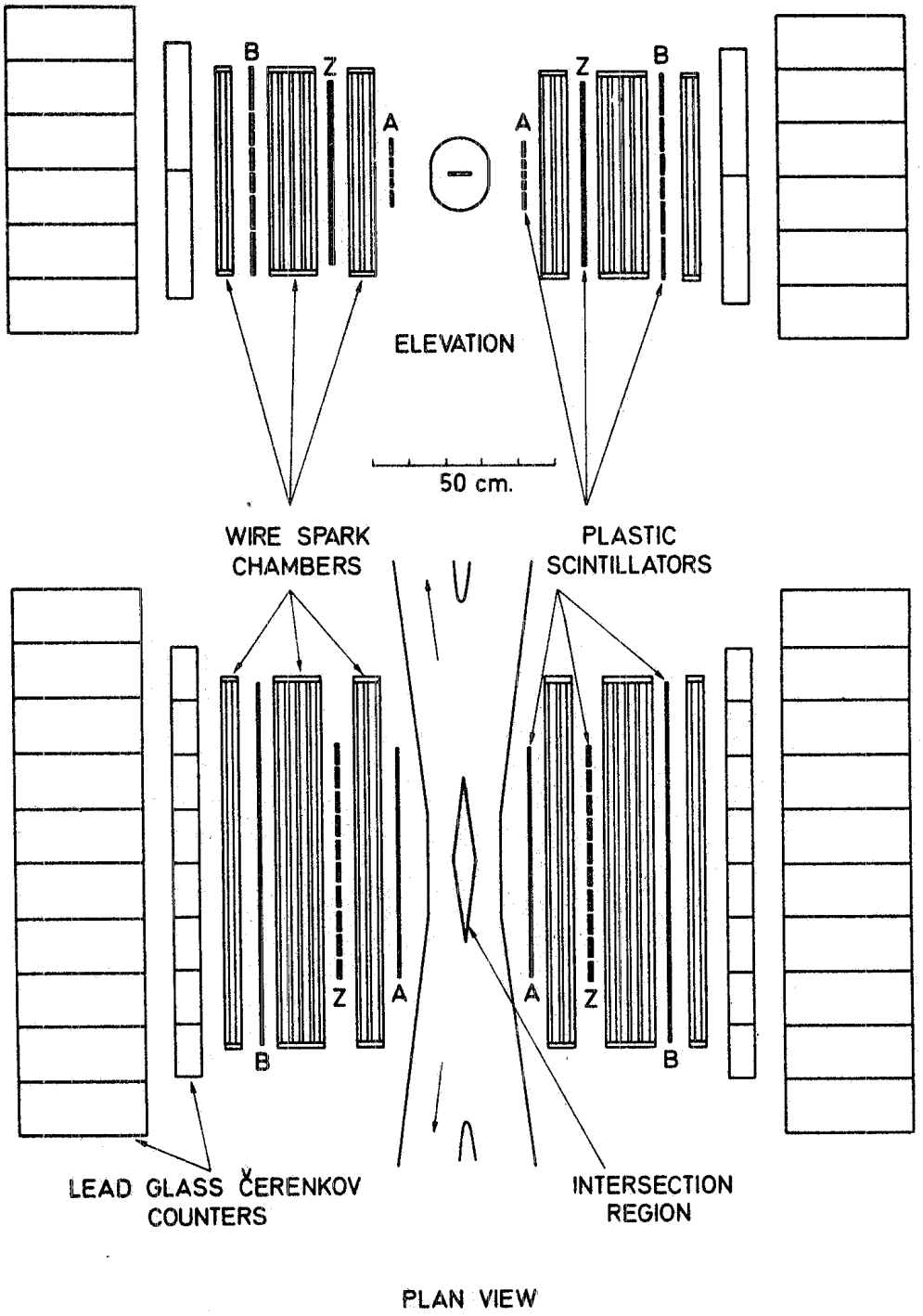

FIG. 1 - The π^o detector of CCR group (Reference 3).

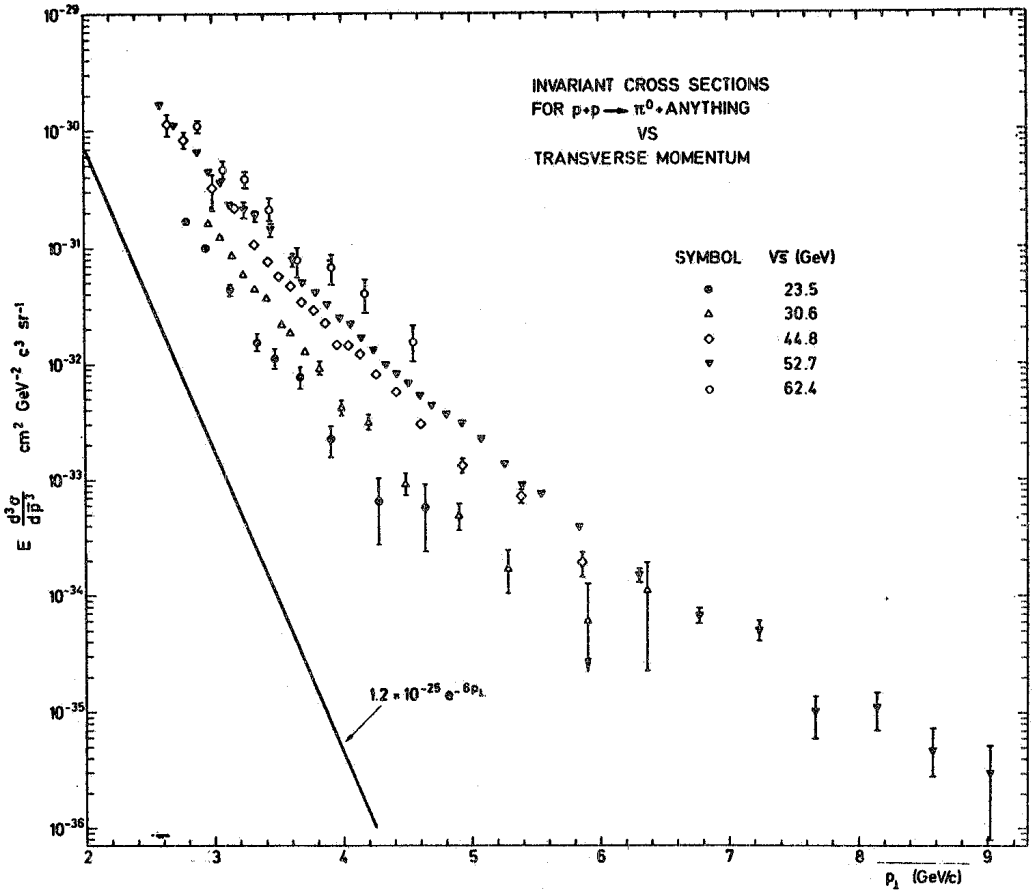

FIG. 2 - The transverse momentum dependence of the invariant cross-sections for inclusive π^0 production at various center of mass energies. The solid line is the extrapolation of the exponential fall-off at low $P_\perp$ (3).

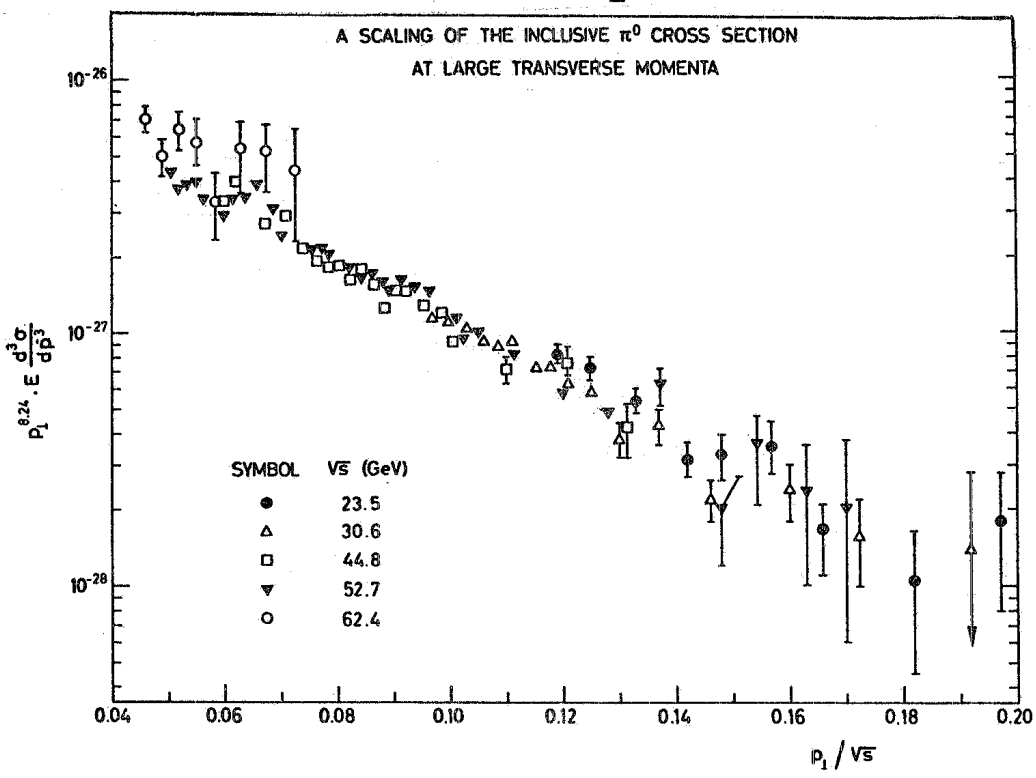

FIG. 3 - Scaling of the inclusive π^0 cross section at large $P_\perp$ (CCR data(3)).

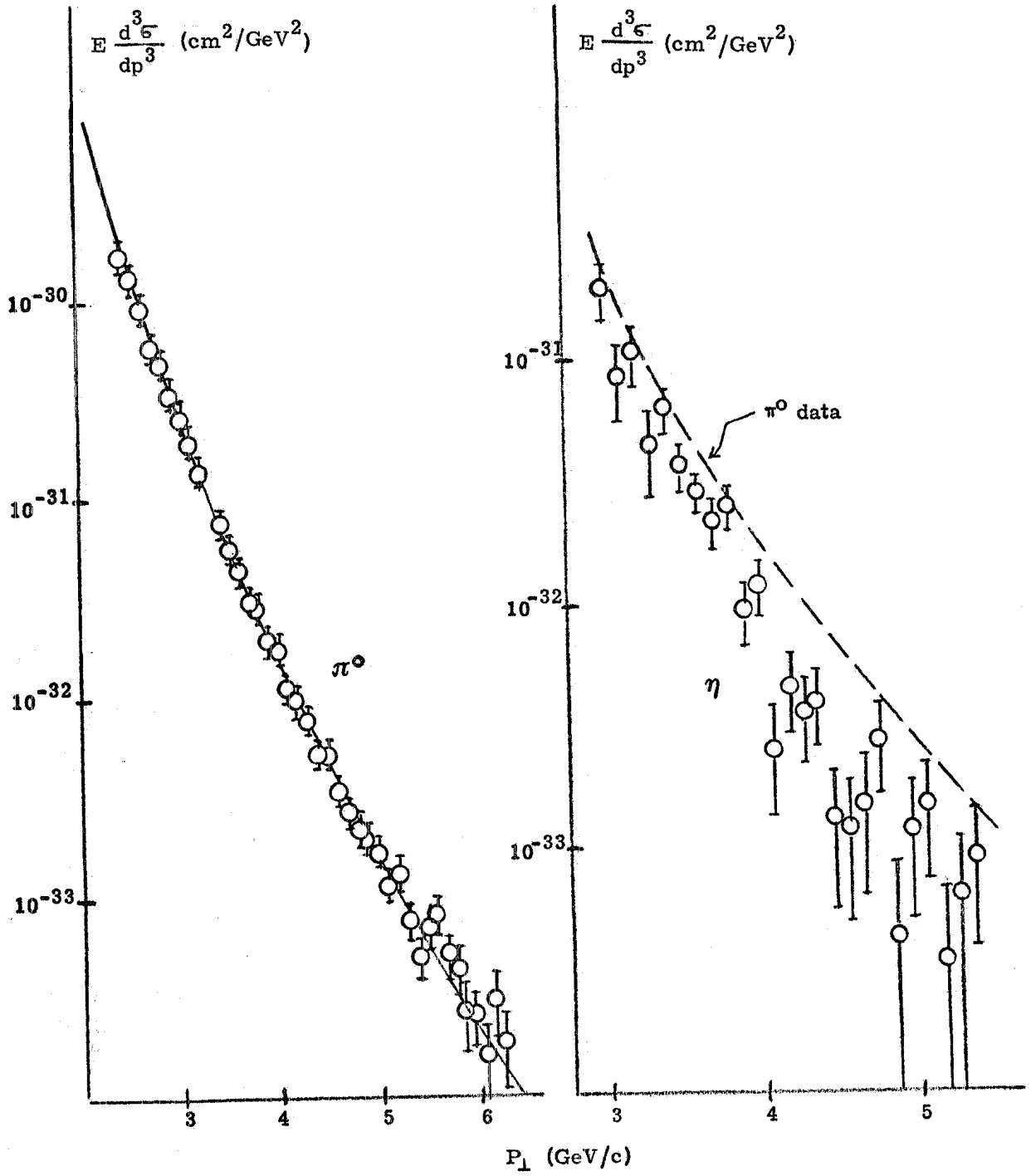

FIG. 4 - Results on π^0 and η cross sections as a function of $P_\perp$ at $\sqrt{s}$ = 52.7 GeV (CCRS, ref. 5). The broken curve shown in the η-data is the same curve fitting the π^0 data.

The British-Scandinavian Collaboration has studied extensively at the ISR the inclusive production cross section at high $P_\perp$ of different charged particles[6]. They have used a wide angle spectrometer as shown in Fig. 5. Pions, kaons, protons (or antiprotons) were identified by means of

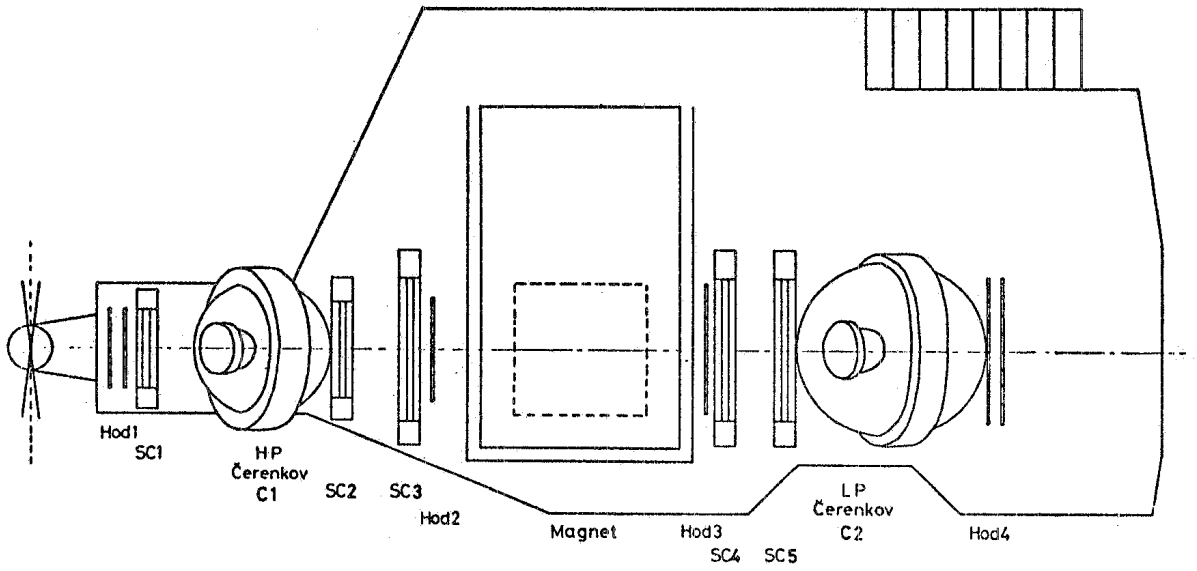

FIG. 5 - Layout of the British-Scandinavian spectrometer[6].

two threshold gas Cerenkov counters. Particle momenta were measured by a system of scintillation hodoscopes, wire spark chambers and an one meter long bending magnet. The invariant cross sections for π^+, π^-, K^+, K^-, p and $\bar{p}$ are shown in Fig. 6 for $\sqrt{s} = 53$ GeV and $\theta_{CM} = 89.0^\circ$. To illustrate the energy dependence, the cross sections as a function of $P_\perp$ for π^+, K^+ and p at different $\sqrt{s}$ are plotted in Fig. 7, 8 and 9. It is seen that the cross-section increases with increasing $\sqrt{s}$ but this effect is not so strong in the kaon data and it is hardly present in the proton data. In other words, the particle composition at large $P_\perp$ is energy dependent in the ISR energy range. At $\sqrt{s} =$ = 53 GeV, the relative abundance of π^+, π^-, K^+, K^-, p and $\bar{p}$ as a function of $P_\perp$ is shown in Fig. 10. At small $P_\perp$, 90% of the charged particles are pions. However the contribution of the heavier particles rises as a function of $P_\perp$ up to $P_\perp \approx 1.5$ GeV/c where about 40% of the particles are heavier than pions. Above 1.5 GeV/c the contribution from kaons and nucleons roughly levels off.

The data from Fermi Lab. are consistent in the general features with those from the ISR. Fig. 11 shows the focusing spectrometer of the Chicago-Princeton group at the Fermi-Lab.[7]. The particle identification was done by the threshold Cerenkov counters and the momenta were measured by the system of counter hodoscopes and magnets. The production angle chosen in the Laboratory system (77 mr) was such that the detected particles were produced at $\theta_{CM} \approx 90^\circ$. The inclusive invariant π^- cross section per effective nucleon in p-W collision[8], plotted against $P_\perp$ at 200, 300 and 400 GeV incident proton momenta, is shown in Fig. 12. As in the CCR π^0 data, the energy dependence becomes larger as $P_\perp$ increases. In Fig. 13, the invariant cross section in a logarithmic scale is plotted against the scaling variable $x_\perp = 2P_\perp / \sqrt{s}$. One sees that for $x_\perp \gtrsim 0.4$, the data enter into a scaling region and the invariant cross section can be written in the form

$$E \frac{d\sigma}{d^3 p} = g(s)\, f(x_\perp)$$

where g(s) is some function of s and $f(x_\perp)$ is a function of the scaling variable $x_\perp$. By fitting these data to the expression

(2)
$$E \frac{d\sigma}{d^3 p} = s^{-n} e^{-a x_\perp}$$

the authors of ref. (7) obtained: $n = 5.4 \pm 0.2$ and $a = 36.0 \pm 0.4$. Observing that these values were

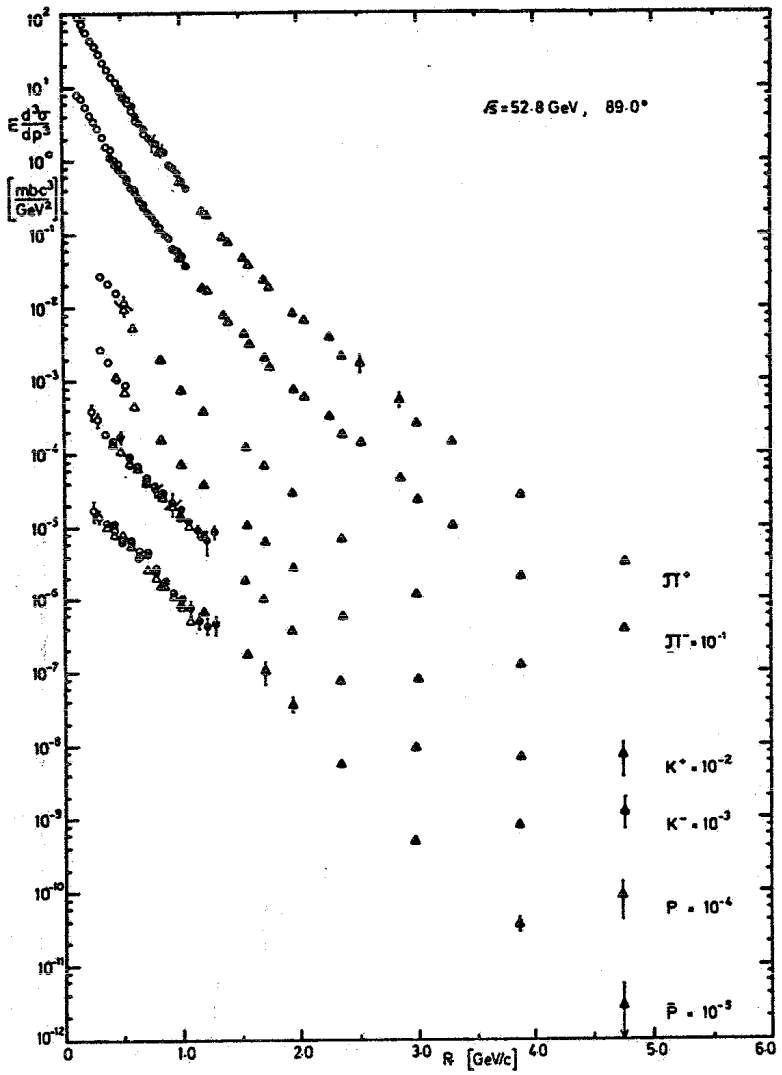

FIG. 6 - The invariant inclusive cross sections for π^+, π^-, K^+, K^-, p and $\bar{p}$ at $\sqrt{s}$ = 52.8 GeV and $\theta_{cm} = 89^o$ as a function of $P_\perp$ (ref. 6).

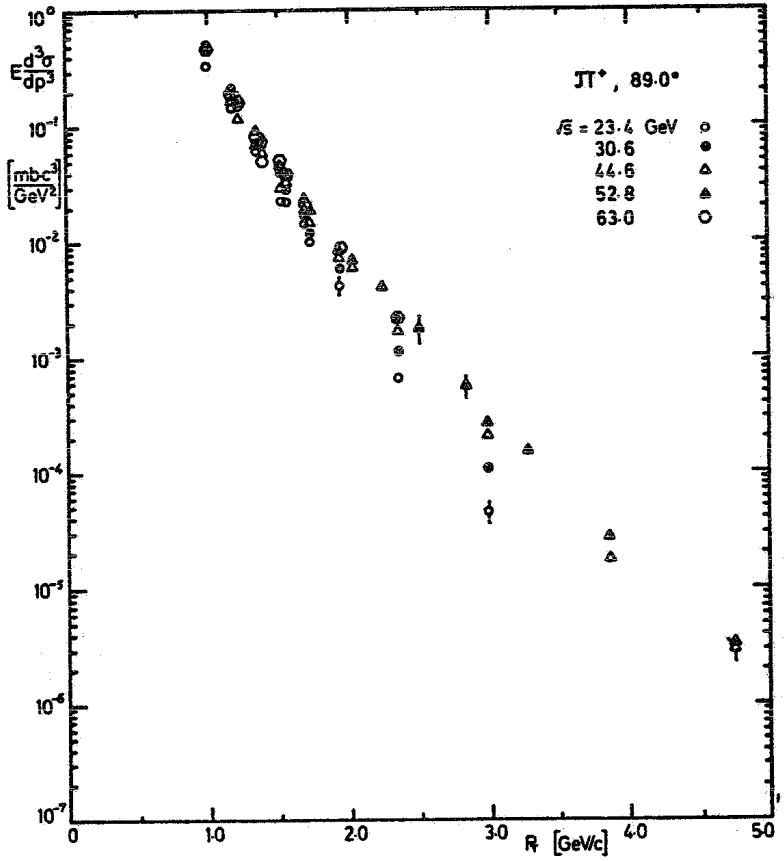

FIG. 7 - The invariant inclusive cross sections for π^+ at 5 different ISR energies at $\theta_{cm} = 89^o$ (ref. 6).

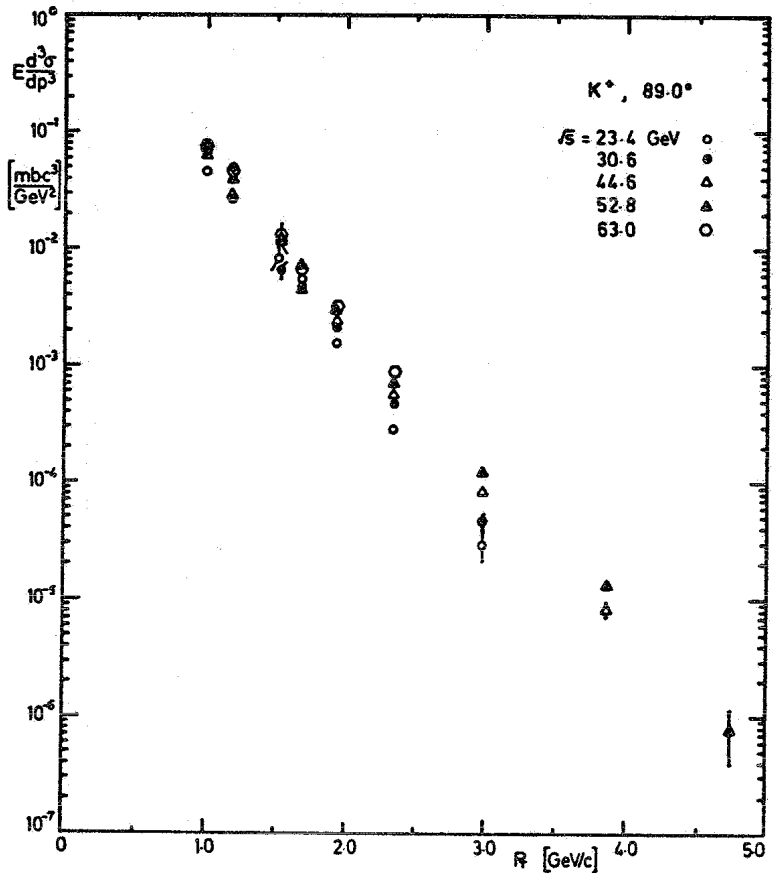

FIG. 8 - The invariant inclusive cross sections for K^+ at 5 different ISR energies at $\theta_{cm} = 89^o$ (ref. 6).

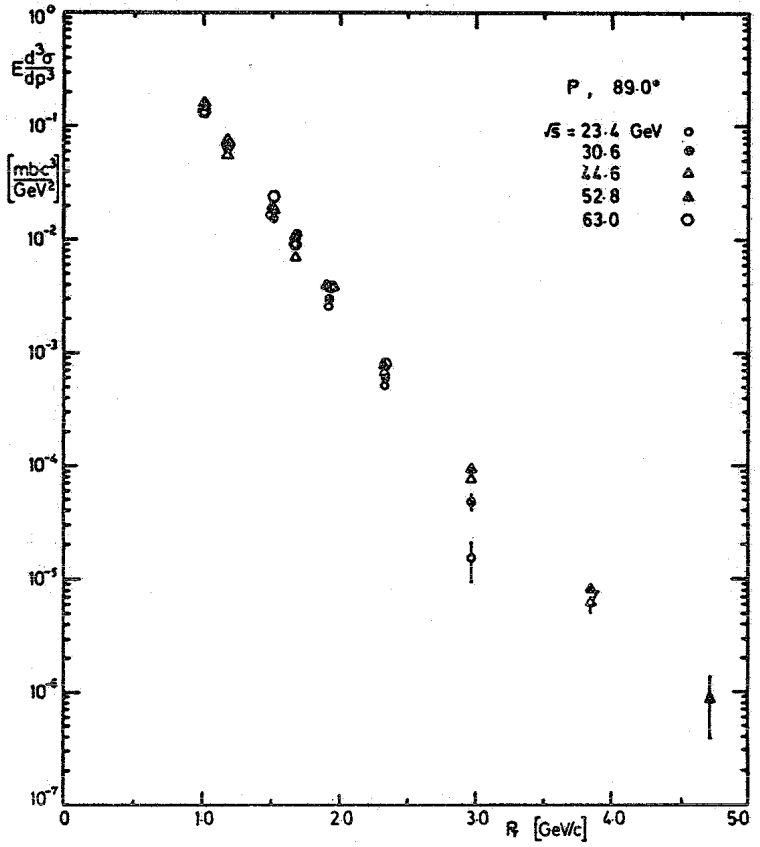

FIG. 9 - The invariant inclusive cross sections for protons at 5 different ISR energies at $\theta_{cm} = 89^o$ (ref. 6).

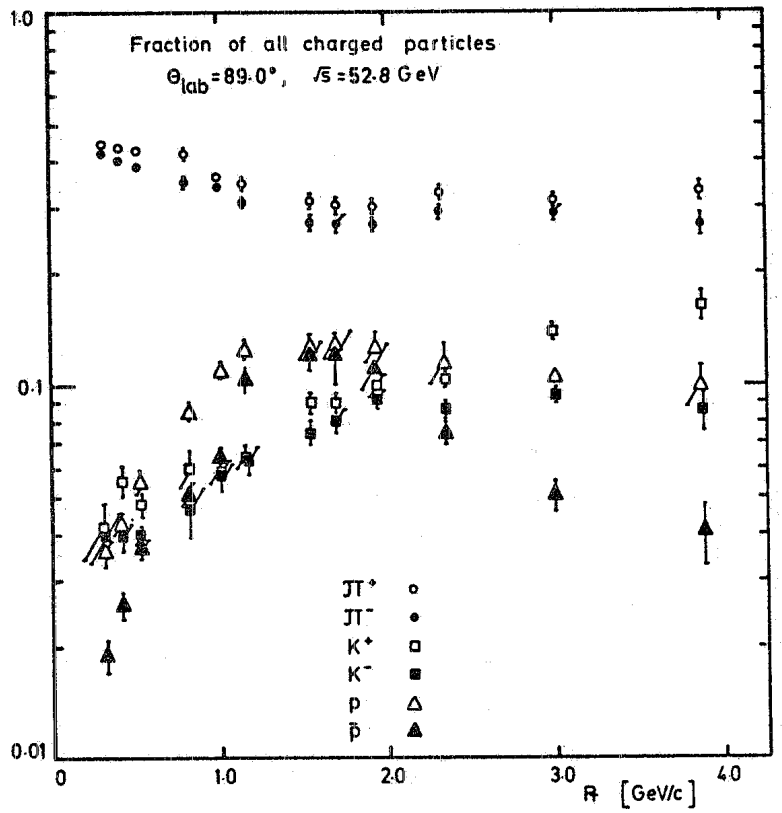

FIG. 10 - Fraction of all charged particles at $\sqrt{s}$ = 52.8 GeV and $\theta_{cm} = 89^{o}$ (ref. 6).

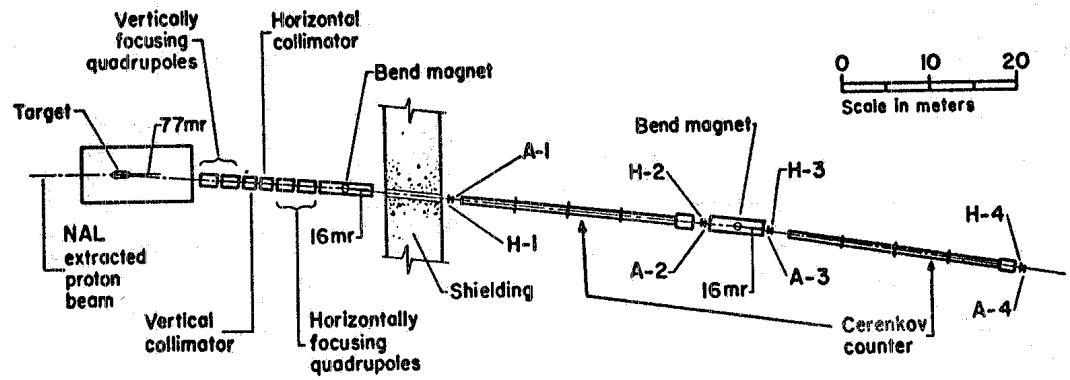

FIG. 11 - Experimental set up of the Chicago-Princeton group at Fermi Lab. (ref. 7).

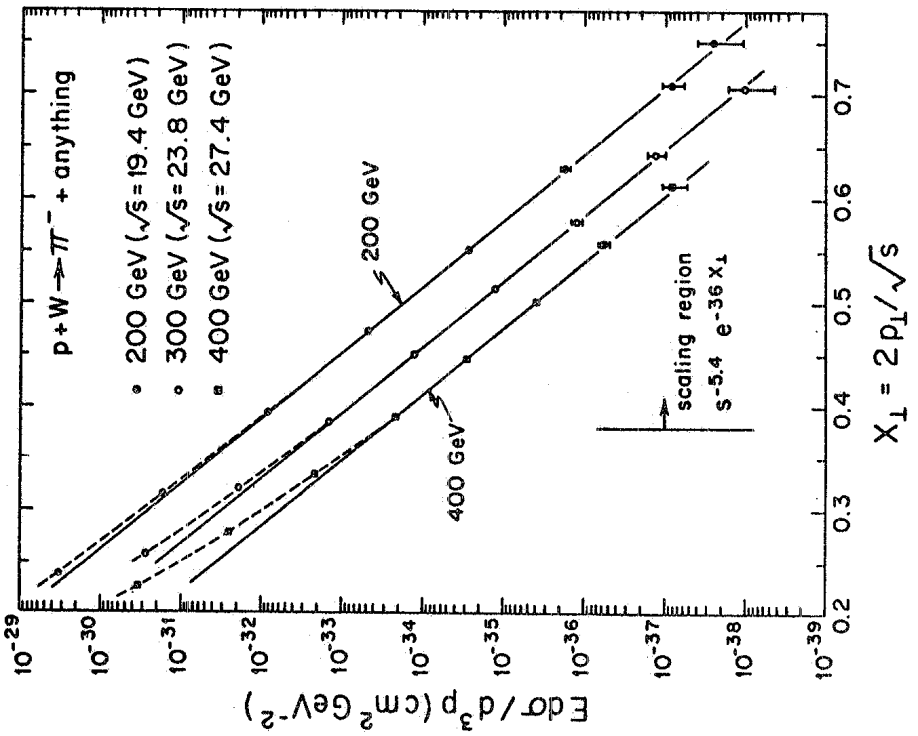

FIG. 13 - Inclusive invariant cross section per effective nucleon for π^- produced at $\theta_{cm} \approx 90^o$ in p - W collisions, as a function of $x_\perp$ for laboratory momenta between 200 GeV/c and 400 GeV/c (ref. 7).

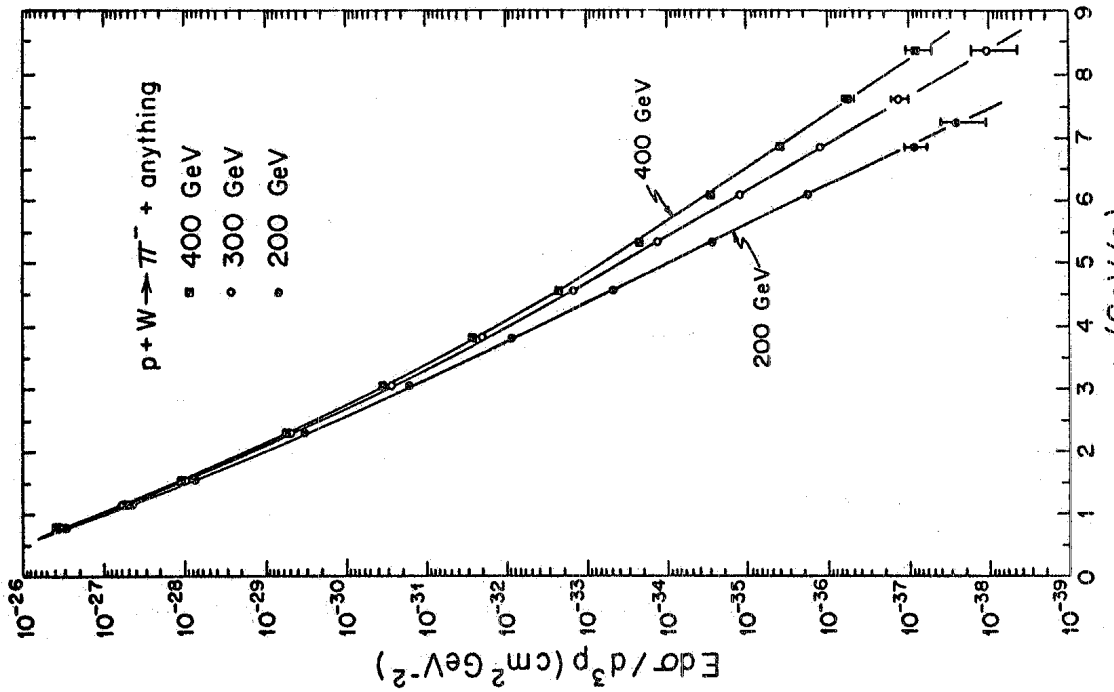

FIG. 12 - Inclusive invariant cross section per effective nucleon for π^- produced at $\theta_{cm} \approx 90^o$ in p - W collisions as a function of $P_\perp$ for laboratory momenta between 200 GeV/c and 400 GeV/c (ref. 7).

different from the fits made by the CCR group (formula (1)), and that all data indicated that neutral and charged pions behave very much in the same way, the Chicago Princeton group calculated that the fitting parameters could depend on $x_\perp$. They plotted the values of n obtained from their Be data as a function of $x_\perp$ (Fig. 14). This figure suggests that the fitted parameters depend on the region of phase space in which one works. In this context, large values of $x_\perp$ are not necessarily more desirable when searching for asymptotic properties of the data because they are near the boundary of phase space.

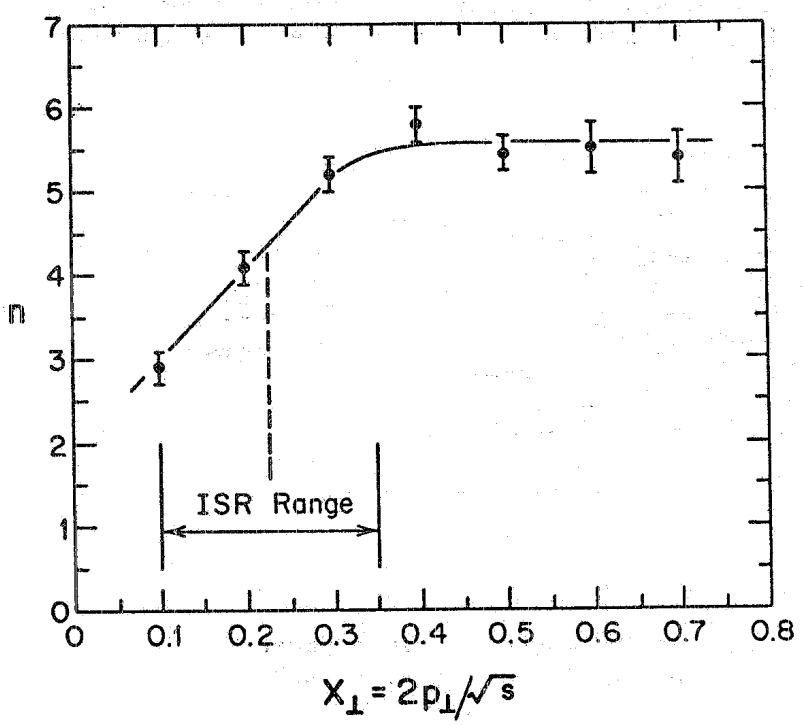

FIG. 14 - The exponent n (formula (2) in the text) versus $x_\perp$ from the average $\pi^\pm$ cross sections of the Chicago-Princeton data[7].

To summarize the above observations, the main features seen in the inclusive hadron production at large $P_\perp$ and large angles are as follows:

a) The inclusive pion cross section shows power law dependence on $P_\perp$ at large $P_\perp$ and this suggests point like interactions. However one needs ad-hoc model to predict the value of the exponent[1,c].

b) At large $P_\perp$, the invariant cross section grows with s and it can be put into a scaling form both in the variables $x_\perp$ and s and in the variables $P_\perp$ and $x_\perp$. The parameters of these fits, however, depend on the region of phase space in which the fits are performed.

c) Although an increased production at large $P_\perp$ is present also for particles heavier than pions, the energy dependence of the cross section is different, so that the particle composition for $P_\perp \gtrsim 0.5$ GeV/c varies quite appreciably with s. Very qualitatively, one can say that above $P_\perp \approx 0.5$ GeV/c, the contribution of particles heavier than pions grows from about 10% to about 40% but for $P_\perp$ about 3 or 4 GeV/c, and for particles heavier than kaons, the contribution is still varying fast with energy and $P_\perp$ even at ISR energies. This effect of course can be due to phase space limitations.

2.- PARTICLE CORRELATIONS IN LARGE $P_\perp$ EVENTS.-

If an event contains a large $P_\perp$ secondary the other particles produced in the same interaction must be emitted in such a way that the overall transverse momentum be balanced to zero. This constraint, however, can be met in many ways. For instance, transverse momentum could either be balanced by only one particle of large $P_\perp$ emitted opposite to the first one, or it could be balanced by many soft particles. In addition, in both of these cases the particles could be emitted anywhere in longitudinal phase space. With reference to the experiments discussed in Section 1, in which the large $P_\perp$ triggering particle was detected around 90° in the center of mass system, the associated particles could be emitted also around 90° (and opposite in azimuthal angle) or they could be emitted at any polar angles, even at small angles with respect to the beams (but of course opposite in azimuthal angle). Therefore the study of the multiplicity of particles produced in association with a large $P_\perp$ particle and of their angular distributions is of great interest.

A number of experiments have faced this problem at the ISR, where one works in the center of mass system and one can achieve more easily a large efficiency for detection of all produced particles. The Pisa-Stony Brook (PSB) Collaboration has measured the charged particle multiplicities associated with large transverse momentum photons (in practice carrying the total energy of

the parent π^o)[9]. Fig. 15 shows their 4π counter hodoscope system and the lead glass Cerenkov counters for detecting photons at $\theta_{CM} = 90^o$. The multiplicity and angular distribution of charged particles are measured with hodoscopes $H_2\theta$, $H_4\theta$ and L. The outer layer of the L hodoscope together with $H_2\theta$ and $H_4\theta$ gives 43 polar angle (θ) bins, each of which has four azimuthal (ϕ) bins (see Fig. 16). These hodoscope cover about 80% of the total solid angle. The inner layer of the L hodoscope provides 20 ϕ bins for detail study of the azimuthal distribution in the central region (see insert in Fig. 15). The hodoscopes H_1,H_2, H_3, H_4 and TB are used to trigger on beam-beam interactions.

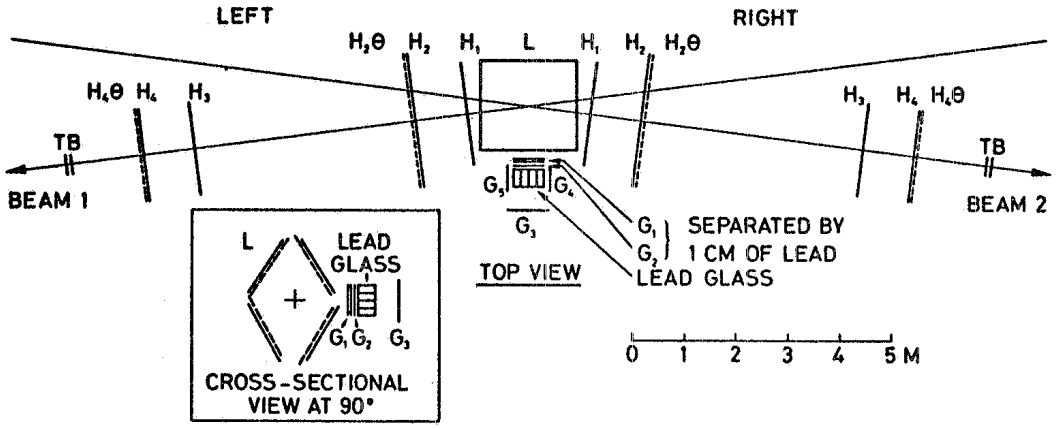

FIG. 15 - Experimental set up of the PSB Collaboration, with a photon detector at 90°. H_1, H_2, $H_2\theta$, H_3, H_4, $H_4\theta$ and TB are counter hodoscopes[9].

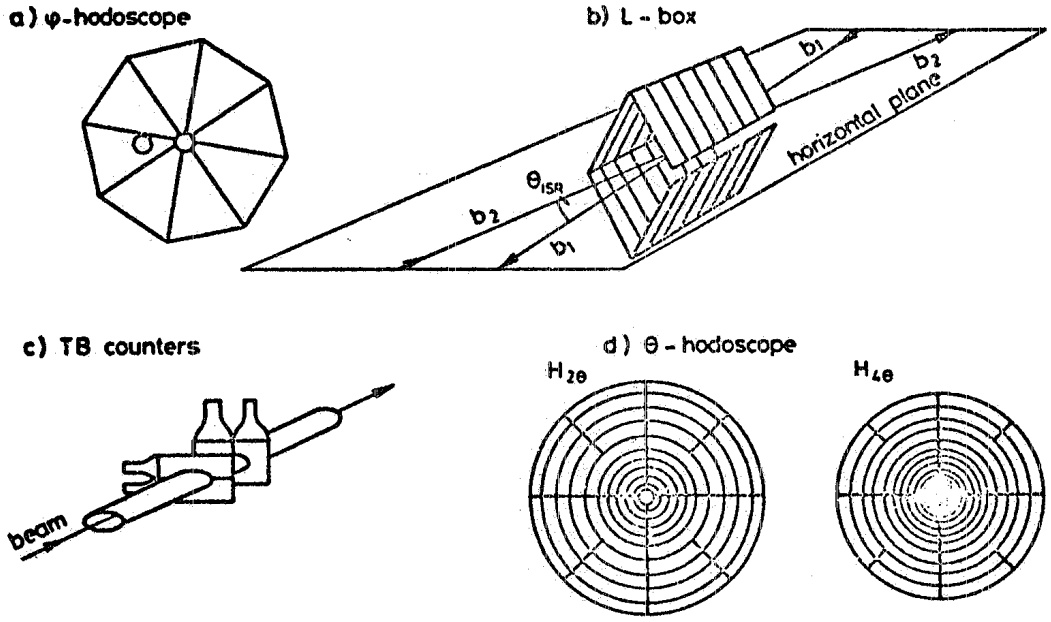

FIG. 16 - Sketch of hodoscopes of the PSB experiment[9], showing the structure of the detectors into bins of polar and azimuthal angles.

The average total multiplicity of charged particles[x] as a function of $P_\perp$ of the photon at 90° is plotted in Fig. 17. The data were taken at $\sqrt{s} = 53$ GeV, and they are normalized to the multiplicity in the lowest $P_\perp$ bin. The normalized multiplicity first increases almost linearly with $P_\perp$ and than starts to drop at $P_\perp \simeq 3$ GeV/c. From small $P_\perp$ to 3 GeV/c, the increase is about 13%.

The PSB Collaboration has also studied the $\eta(\eta = -\ln \tan(\theta/2))$ distribution of the charged secondaries for different intervals of $P_\perp$. As shown in Fig. 18, these plots are devided into two hemispheres centered on the directions toward and away from the photon detector. Several interesting features are obtained from these plots. For both toward and away hemispheres, at small forward angles ($|\eta| \gtrsim 3$) the partial multiplicity falls linearly with increasing $P_\perp$. At large angles ($\eta \approx 0$) there is no significant increase of partial multiplicity as $P_\perp$ increases on the toward hemisphere, but on the away hemisphere the partial charged multiplicity grows by 0.7 to 0.8 particles for each GeV/c increase in $P_\perp$. To further illustrate the above observations, Fig. 19 gives the partial multiplicity, normalized to the multiplicity obtained with an inclusive beam-beam trigger, as a function of $P_\perp$ in the interval of $-0.7 < \eta < 0.7$ for two narrow azimuthal angular ϕ-bins centered at $\phi = 25°$ and at $\phi = 180°$. This normalized multiplicity grows approximately linearly with P for the $\phi = 180°$ data but is independent of $P_\perp$ for the $\phi = 25°$ data. Notice that for the $\phi = 180°$ data, the multiplicity does not drop beyond $P_\perp \simeq 3$ GeV/c as in Fig. 17 which includes secondaries emitted at small angles (large $|\eta|$). Since small angle particles are in general very energetic, it is natural to attribute this drop to the effect of energy conservation.

The data shown in Fig. 17 to 19 can be taken as an indication that a "jet" of particles is produced over a broad region of scattering angle ($-3 < \eta < 3$) and opposite in azimuth to the large $P_\perp$ π^0. The azimuthal distribution of particles within the core of this "jet" is studied in Fig. 20 which shows the multiplicity (normalized to the low-$P_\perp$ data) as a function of ϕ in the interval $-0.7 < \eta < 0.7$ for different $P_\perp$ ranges. It can be seen that the azimuthal angular distribution is very broad and is centered at $\phi = 180°$. Of course the azimuthal asymmetry is largest for the largest $P_\perp$ bin. The width of the distribution is about $\Delta\phi = 120°$ at half height while the angle subtended by the photon detector is only $\Delta\phi = 30°$.

Although the data presented from Figs. 17 to 20 are suggestive of a possible jet of particles emitted in association with a large $P_\perp$ trigger in such a way as to balance its transverse momentum, the evidence for such an effect is by no means conclusive. To get further insight into this phenomenon, one can argue as follows: suppose that the large $P_\perp$ particle and its associated jet are produced by a point like interaction between the constituents of the two primary particles, and this interaction proceeds to a first approximation independent of the rest of the interactions. In this case one might expect to find in the center of mass system a roughly back-to-back correlation in real space between the large $P_\perp$ particle and the recoiling jet. They would however be surperimposed over other particles produced as in a "normal" interaction. Such possibility has also been considered in a number of quark-or parton-like models[1, c]. In order to study this effect experimentally, the obvious approach is to study events in which a large $P_\perp$ particle is emitted at an angle different from $\theta_{CM} = 90°$ and to see whether the associated jet moves to the opposite polar angle. A study of this type was done by the PSB Collaboration by moving the photon detector to a forward $\theta_{CM} = 17.5°$ ($13.6° < \theta_{CM} < 21.3°$) which corresponds to $\eta = 1.89 \pm 0.22$[10]. Fig. 21 shows the total associated charged multiplicity as a function of $P_\perp$ of the detected photon at $\theta_{CM} = 17.5°$. The data for $\theta_{CM} = 90°$ is also shown for comparison. The multiplicity is normalized to the lowest bin in $P_\perp$ ($0 < P_\perp < 0.5$ GeV/c). One sees that the multiplicities associated with photons at $\theta_{CM} = 17.5°$ rise less rapidly with $P_\perp$ than in the case of $\theta_{CM} = 90°$. One should observe however that by requesting a particle at $\theta_{CM} = 17.5°$ to have large $P_\perp$ one also requests it to have a very large longitudinal momentum (for instance, for $P_\perp = 3$ GeV/c, $P_\parallel = 9$ GeV/c). Therefore energy conservation limits stronghly the growth of the associated multiplicity. One can suspect that if it were not because of this contraint, the multiplicity growth at $\theta_{CM} = 17.5°$ would have been the same as at $\theta_{CM} = 90°$. Fig. 22 gives the ϕ distributions for different η and $P_\perp$ regions for $\theta_{CM} = 17.5°$ of the

---

(x) - All multiplicities quoted in the following from experiments of the PSB Collaboration are defined as number of hits recorded by the counter hodoscopes. No correction has been applied to account for non-complete coverage of solid angle, finite counter resolution, secondary interactions, etc. To a rough approximation, the raw multiplicity is in average 20% higher then the true charged multiplicity.

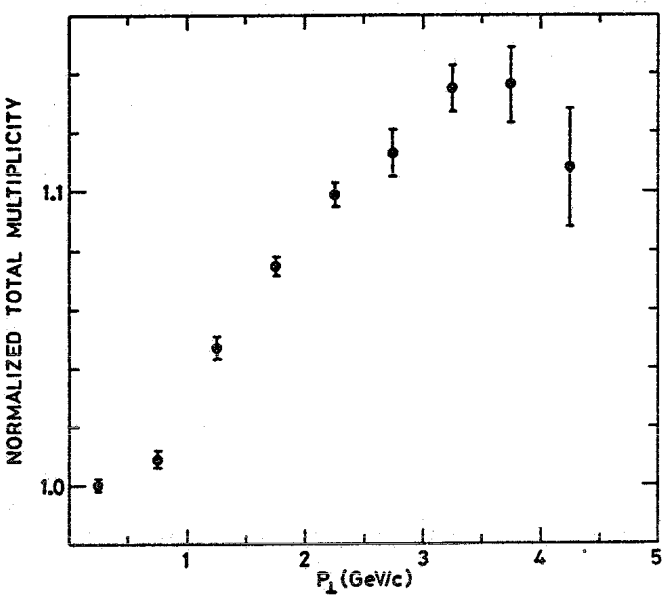

FIG. 17 - Average total charged multiplicity as a function of $P_\perp$ of the photon at 90°. The data are normalized to the multiplicity in the lowest $P_\perp$ bin (ref. 9).

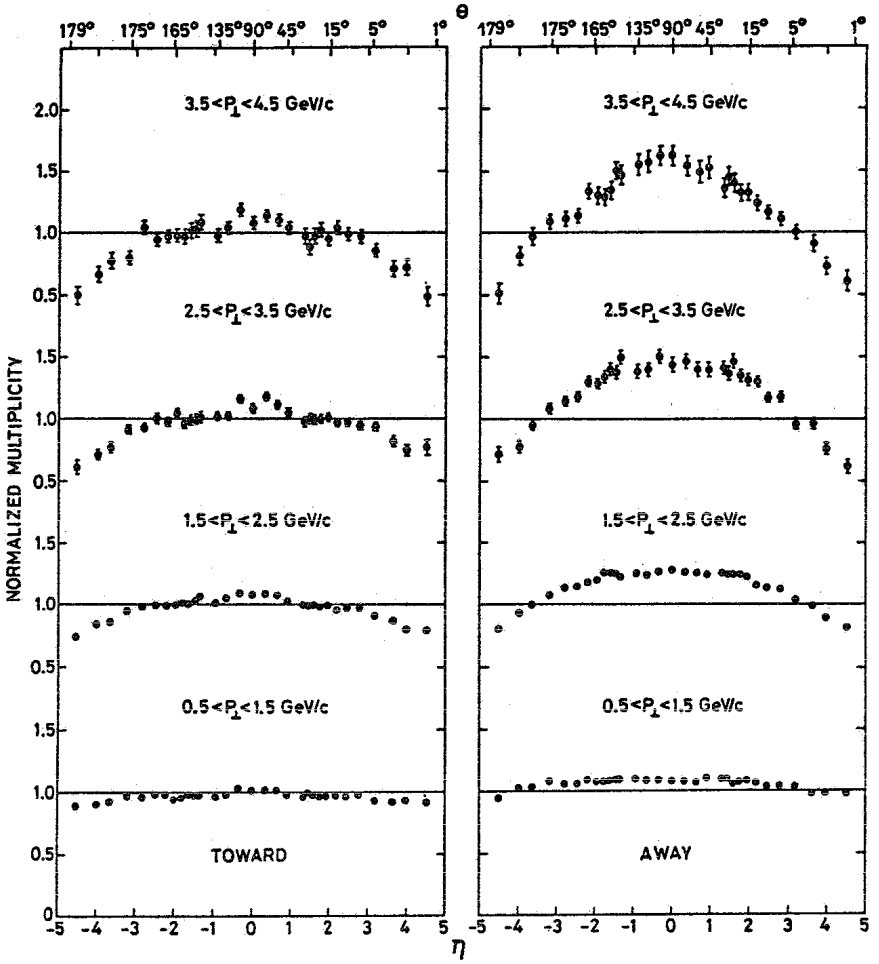

FIG. 18 - Normalized partial multiplicities as a function of $\eta = -\ln \tan \theta/2$ for different $P_\perp$ bins in the two 180° azimuthal regions : the same side and the opposite side of the detected photons (ref. 9). η is an approximation to the particles rapidity $y = \sin h^{-1} \frac{P_\parallel}{\sqrt{P_\perp^2 + m^2}}$, which is valid when $m^2 \ll P_\perp^2$. This condition is well satisfied for the average particle production at the ISR.

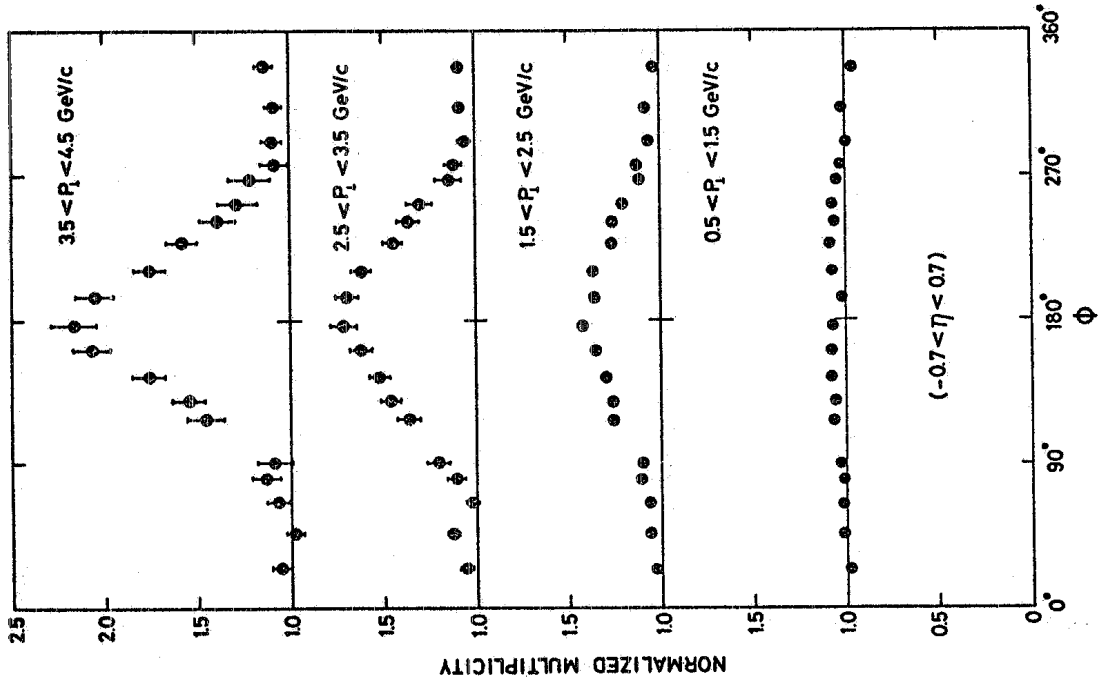

FIG. 20 - Partial multiplicities in the interval $-0.7 < \eta < 0.7$ as a function of the c.m. azimuthal angle ϕ. ϕ is 0° or equivalently 360° for the detected photon. The data are normalized to the lowest $P_\perp$ bin (ref. 9).

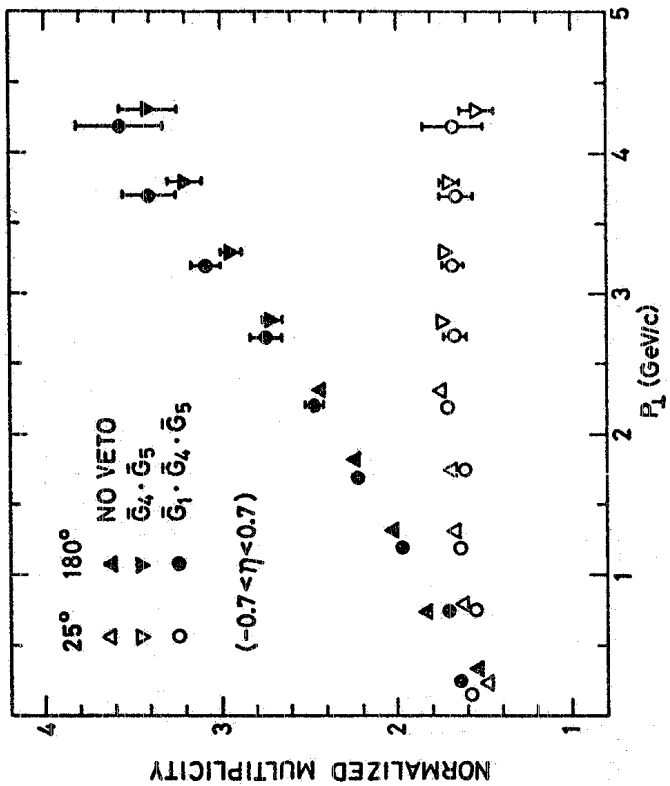

FIG. 19 - Partial multiplicities in the interval $-0.7 < \eta < 0.7$ as a functions of $P_\perp$ for $\phi = 25^\circ$ and $\phi = 180^\circ$. The data are normalized to the multiplicity obtained with an inclusive beam-beam trigger (ref. 9).

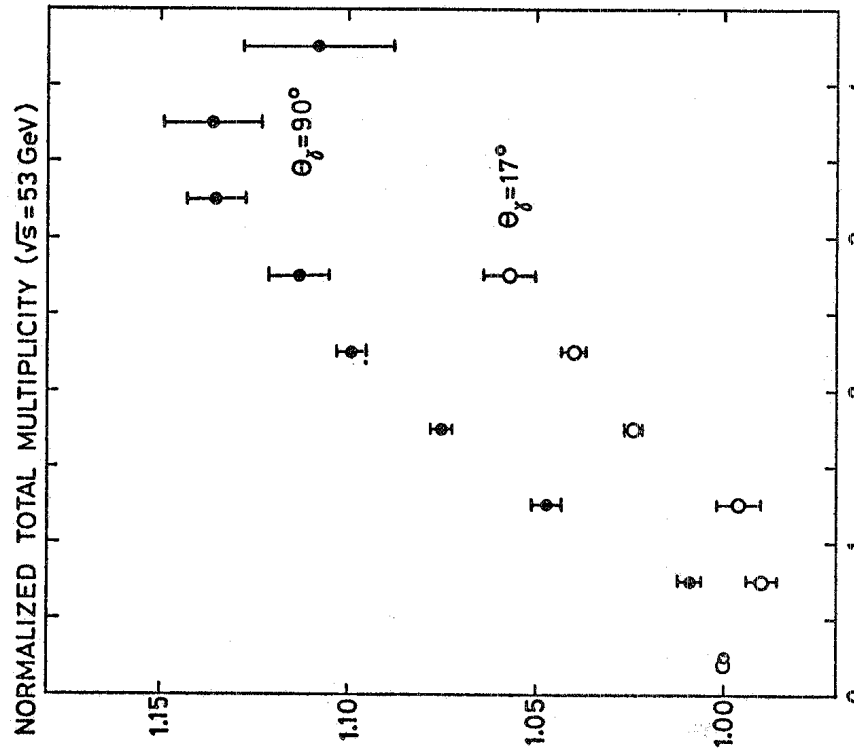

FIG. 21 - Average total multiplicities of charged particles as a function of $P_\perp$ for photons at θ_{cm} = = 90° (full points) and θ_{cm} = 17.5° (open circles). The data are normalized to the multiplicity in the $0 < P_\perp < 0.5$ GeV/c bin (ref. 10).

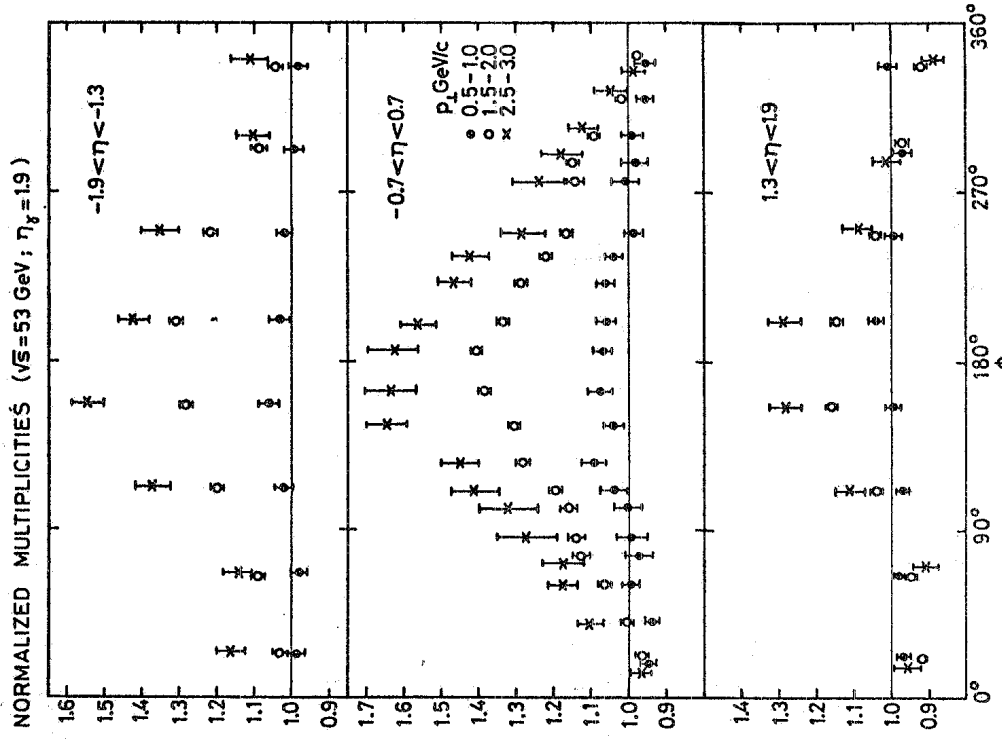

FIG. 22 - Partial multiplicities as a function of azimuthal angle ϕ for different regions of η and $P_\perp$. The detected photon is at ϕ = 0° and θ_{cm} = 17.5°. The data are normalized to the multiplicity in the $0 < P_\perp < 0.5$ GeV/c bin (ref. 10).

detected photon. One notices an excess of particles centered at $\phi = 180^o$ in each of the η-bins. Of course this effect grows with increasing $P_\perp$. One understands in this way that the mechanism by which the transverse momentum is balanced is effective over a very broad range of η. At a first glance, this does not appear to be an indication in favour of the two jets structure. Models can, however, easily account for this affect as the result of the longitudinal motion in the ISR frame of the system of the two constituents, which are the parents of the large $P_\perp$ secondary[9].

For a detailed comparison of the data of $\theta_{CM} = 17.5^o$ and $\theta_{CM} = 90^o$, Fig. 23 shows the η-distribution for different $P_\perp$ ranges, and for secondaries in the hemispheres toward and away of the detected photon. For the $\theta_{CM} = 90^o$ data, as seen before, the distribution centers at $\eta = 0$ (η of detected photon is zero). For the $\theta_{CM} = 17.5^o$ data (η of detected photon is 1.9), however, the distributions are not symmetrical around $\eta = 0$ in both hemispheres, but center at $\eta \approx -0.7$. The multiplicity excess is still found mostly in the away hemisphere. These facts check qualitatively with the naive jet picture that we have discussed before but the shift of the multiplicity excess towards the negative η is much smaller than -1.9. One can however again attribute the non-complete shift to energy-momentum conservation.

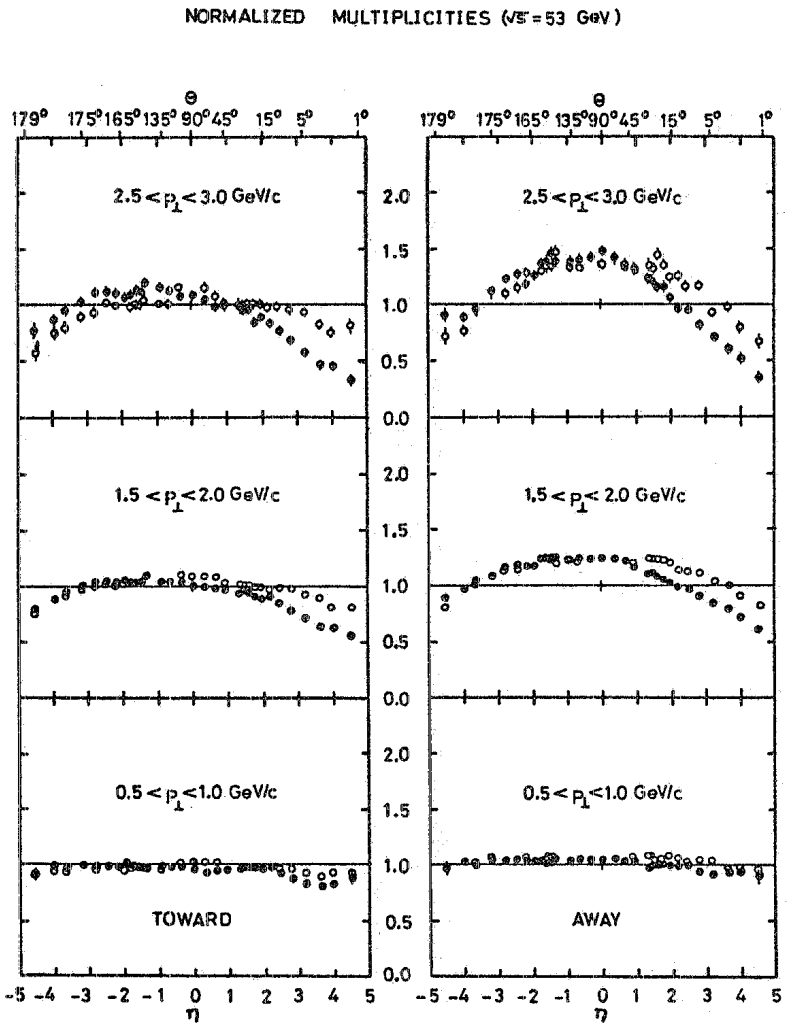

FIG. 23 - Partial multiplicities as a function of η for $\theta_{cm} = 90^o$ (open circles), and $\theta_{cm} = 17.5^o$ (full points), of the photon, for different $P_\perp$ bins and in hemispheres toward and away from photon. The data are normalized to the multiplicity in the $0 < P_\perp < 0.5$ GeV/c bin[10].

After adopting tentatively the two-jet picture, the PSB Collaboration has tried to single out from their 90^o data the jet multiplicity as a function of the photon transverse momentum[11]. The assumption was made that the large $P_\perp$ event is made out of a photon-jet pair of zero total transverse momentum and of total energy $2P_\perp$, superimposed on a normal event of energy $w = \sqrt{s - 2P_\perp}$. Next, the angular distribution and average multiplicity of the charged particles in normal events as function of w were separately measured in the same experiment using an inclusive trigger. This kind of "background" could therefore be removed from large $P_\perp$ events and the multiplicity of the hypothetical jet could be obtained. The result of this analysis is shown in Fig. 24, where one sees that the same distribution is obtained at all ISR energies. This result is just what one would expect in the two-jet picture. One also finds that the jet multiplicity grows with the jet energy at rate of about 0.8 particles/GeV.

Also the Aachen-CERN-Heidelberg-Munich (ACHM) Collaboration has studied at the ISR high energy proton-proton interactions in which a large $P_\perp$ π^o is produced. They use two large streamer chambers surrounding an interaction region for detecting charged particles, and a lead-glass Cerenkov counter for the π^o (see Fig. 25). The chambers are triggered by a coincident signal among scintillator hodoscopes on each downstream arm and the lead glass Cerenkov counter. The distributions of char-

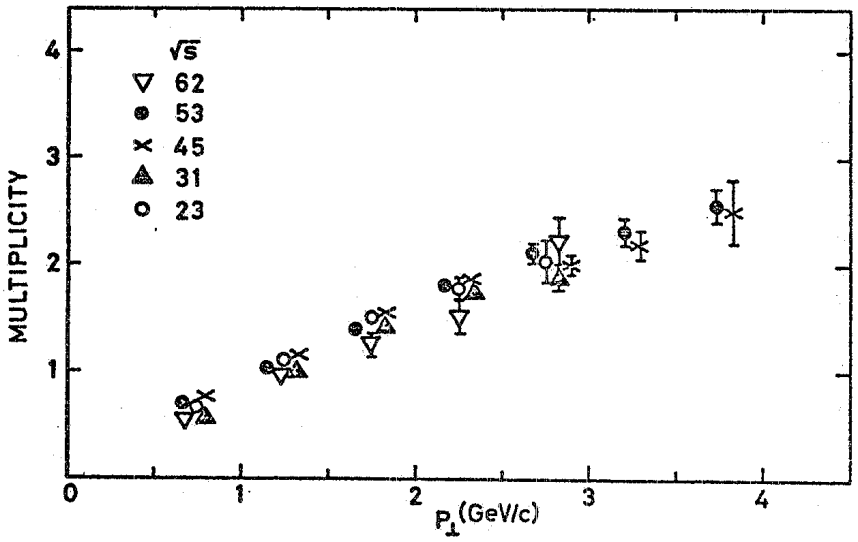

FIG. 24 - Jet multiplicity, derived as explained in the text, as a function of the jet transverse momentum for $\sqrt{s}$ from 23 to 62 GeV (ref. 11).

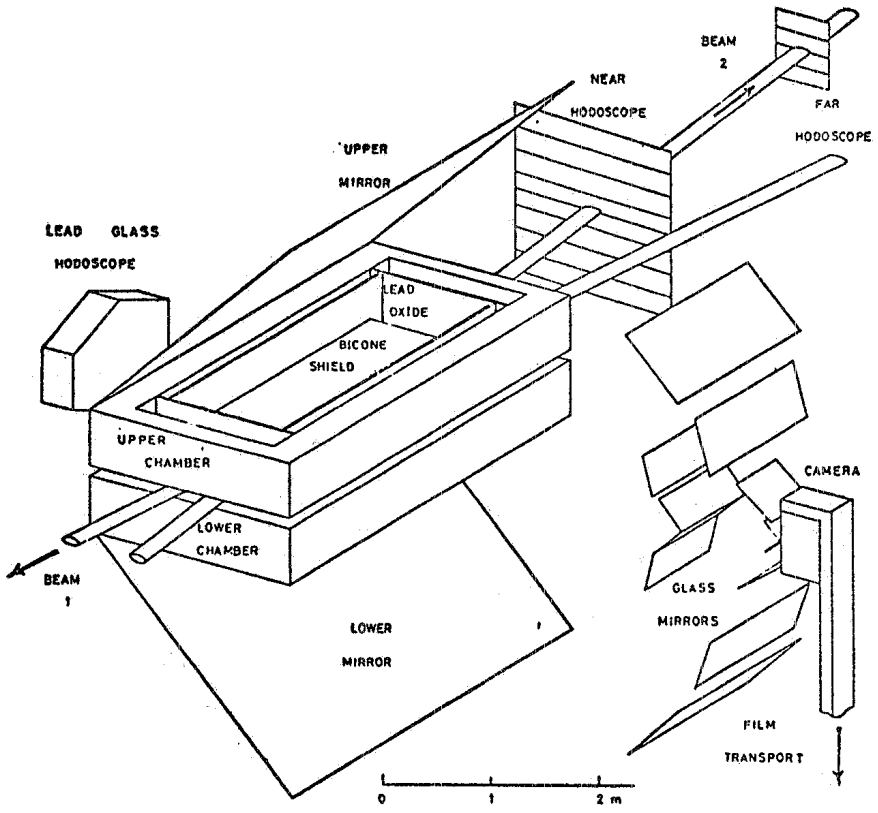

FIG. 25 - Experimental set-up of the Aachen-CERN-Heidelberg-München collaboration (ref. 12).

ged particles produced in association with a π^o detected at $\theta_{CM} = 90^o$ and vertically centered on the beam level were studied in detail for $\sqrt{s} = 53$ GeV[12]. Fig. 26 gives such distributions as a function of η of the secondaries for $P_\perp = 1$ GeV/c and 3 GeV/c of the π^o and for the hemispheres on the opposite and the same sides of the π^o. The general features of these data agree with the Pisa-Stony Brook data i.e. an increase of multiplicity is seen as $P_\perp$ increases for the opposite side but not for the same side. The η distribution of the multiplicity difference between the two hemispheres is also shown at the bottom of Fig. 26.

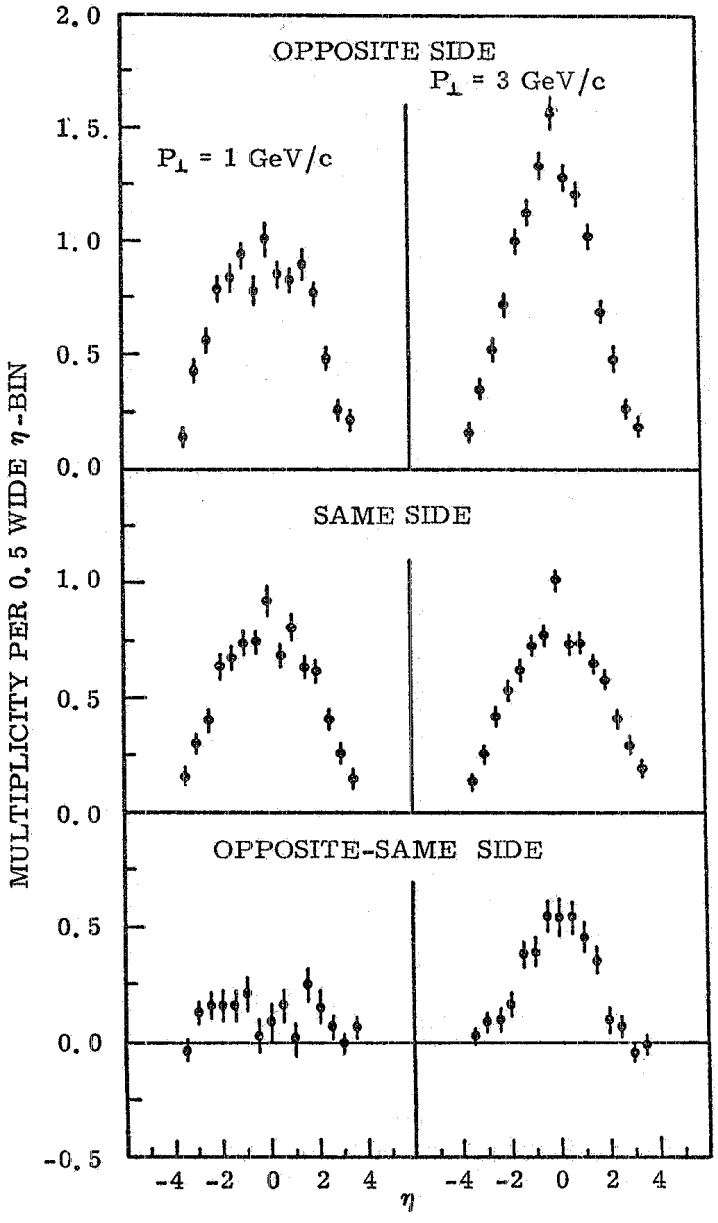

FIG. 26 - Charged multiplicity distribution as a function of η for the opposite and same hemispheres with respect to the large $P_\perp$ π^o. On the left, data for $P_\perp = 1$ GeV/c, and on the right data for $P_\perp = 3$ GeV/c. The π^o is at $-0.3 < \eta < 0.3$. $\sqrt{s} = 53$ GeV. On the bottom of figure, difference between data on the opposite and on the same side (data from ACHM[13]).

Similar to what done by PSB, the ACHM Collaboration has also taken data by moving their π^o detector away from 90°. From Fig. 27 to Fig. 29, one can find their preliminary results for a π^o at $\theta_{CM} = 55^o$, ($\eta = 0.7$), $P_\perp = 3$ GeV/c and $\sqrt{s} = 53$ GeV[13]. Fig. 27 shows the average charged multiplicity as a function of η for different azimuthal intervals. One can see a clear enhancement in the direction roughly opposite to the π^o ($150^o < |\Delta\phi| < 180^o$, and $\eta = -0.7$) and also some enhancement effect in the direction of the π^o itself ($0 < |\Delta\phi| < 30^o$ and $\eta = 0.7$). If one subtracts from Fig. 27 the corresponding distributions obtained with an inclusive beam-beam trigger, one obtains the distributions shown in Fig. 28. One sees some enhancement in the hemisphere $|\Delta\phi| < 90^o$, which is maximum in the direction of the π^o ($|\phi| < 30^o$). Once ϕ enters the opposite hemisphere from the π^o, the enhancement grows as ϕ increases and reaches a maximum at $\phi = 180^o$. The maximum also shifts in η from $\eta \approx 0.7$ at $\phi = 0^o$ to $\eta \sim -0.7$ at $\phi = 180^o$ to result in a back to back effect. In Fig. 29 the charge excess as a function of η is plotted according to different charged multiplicity seen the region of $150^o < \phi < 210^o$. One can conclude that the charge excess and asymmetry in η are contributed both from relatively low multiplicity events as well as from large multiplicity ones. The features seen in Figs. 27 to 29 seem to contribute additional qualitative evidence to the existence of the two jet structure in high $P_\perp$ events. In addition these preliminary data, even within in the limited statistical accuracy, seem to give evidence for structures of narrower η-width and more closely back-to-back correlated, which owing to the more limited angular resolution were not put into evidence by the previously discussed PSB experiment.

Preliminary results from correlation studies with high $P_\perp$ particles rather than π^o have been recently reported by the Daresbury-Illinois-Liverpool-Rutherford (DILR) Collaboration[13]. They have measured the multiplicities and angular distributions of the secondaries for the events

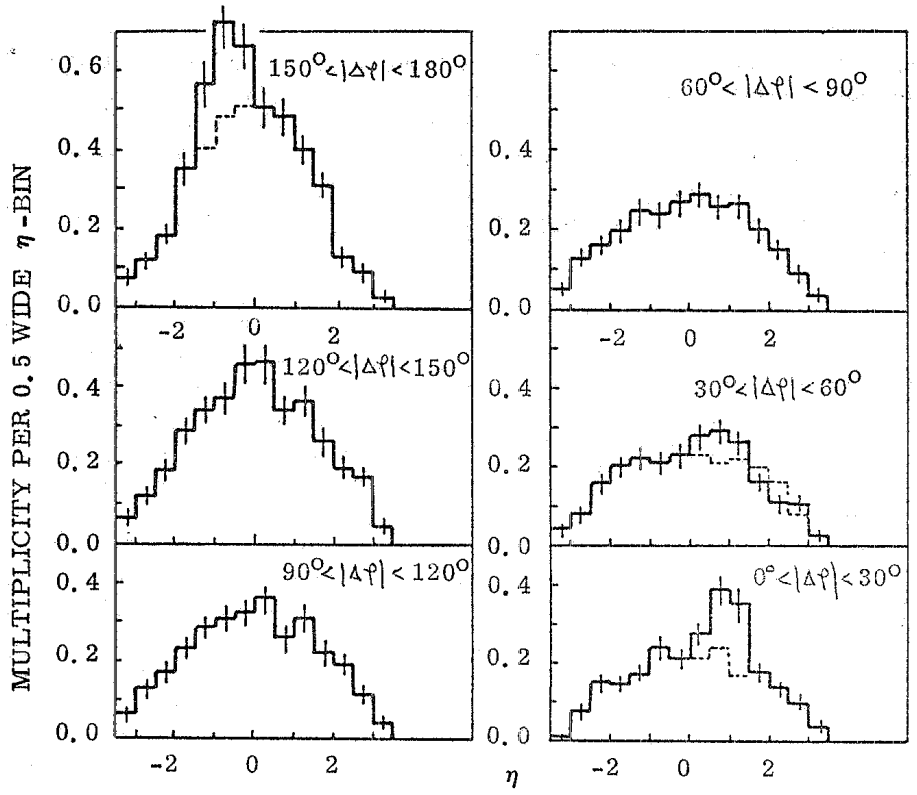

FIG. 27 - Charged multiplicity distribution as a function of η for different azimuthal intervals. The triggering π^0 has $P_\perp \sim 3$ GeV/c and is at $\phi = 0$, $\theta = 55^\circ$ ($\eta \sim 0.7$). $\sqrt{s} = 53$ GeV (data from ACHM, ref. 13). The broken curves show distributions simmetric around $\eta = 0$.

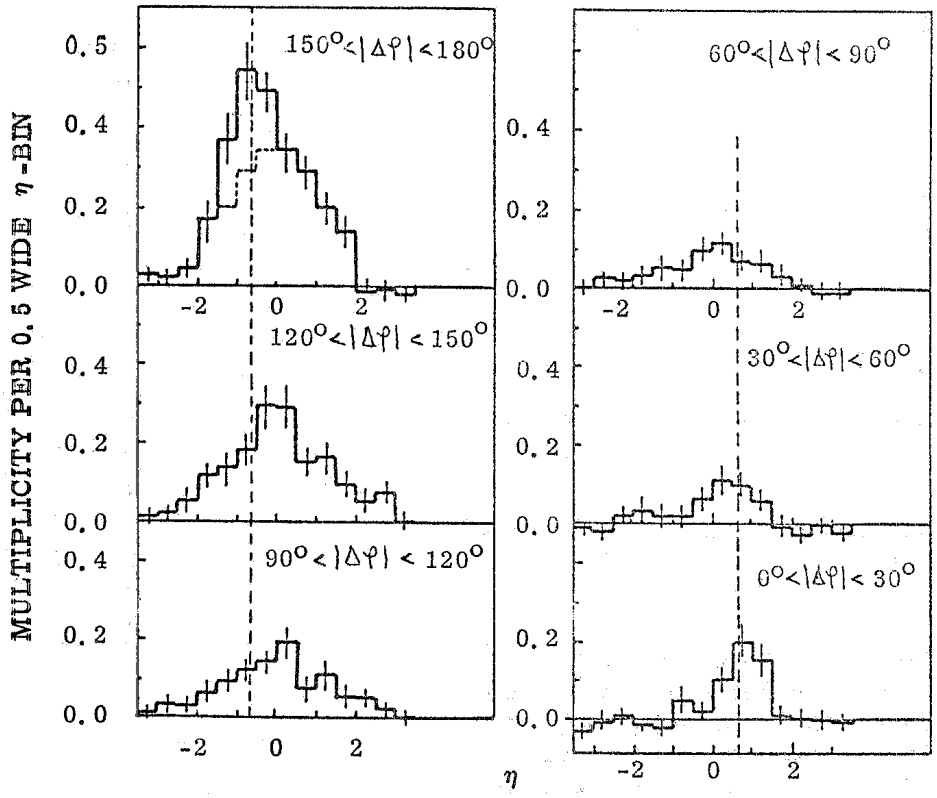

FIG. 28 - Charged multiplicity distribution as a function of η for different azimuthal intervals with respect to the triggering π^0 (at $\phi = 0$, $\theta = 55^\circ$ viz. $\eta \sim 0.7$, and with $P_\perp \sim 3$ GeV/c), after subtraction of the distributions obtained with an inclusive beam-beam trigger. $\sqrt{s} = 53$ GeV (data from ACHM, ref. 13). The broken curve shows a distribution simmetric around $\eta = 0$.

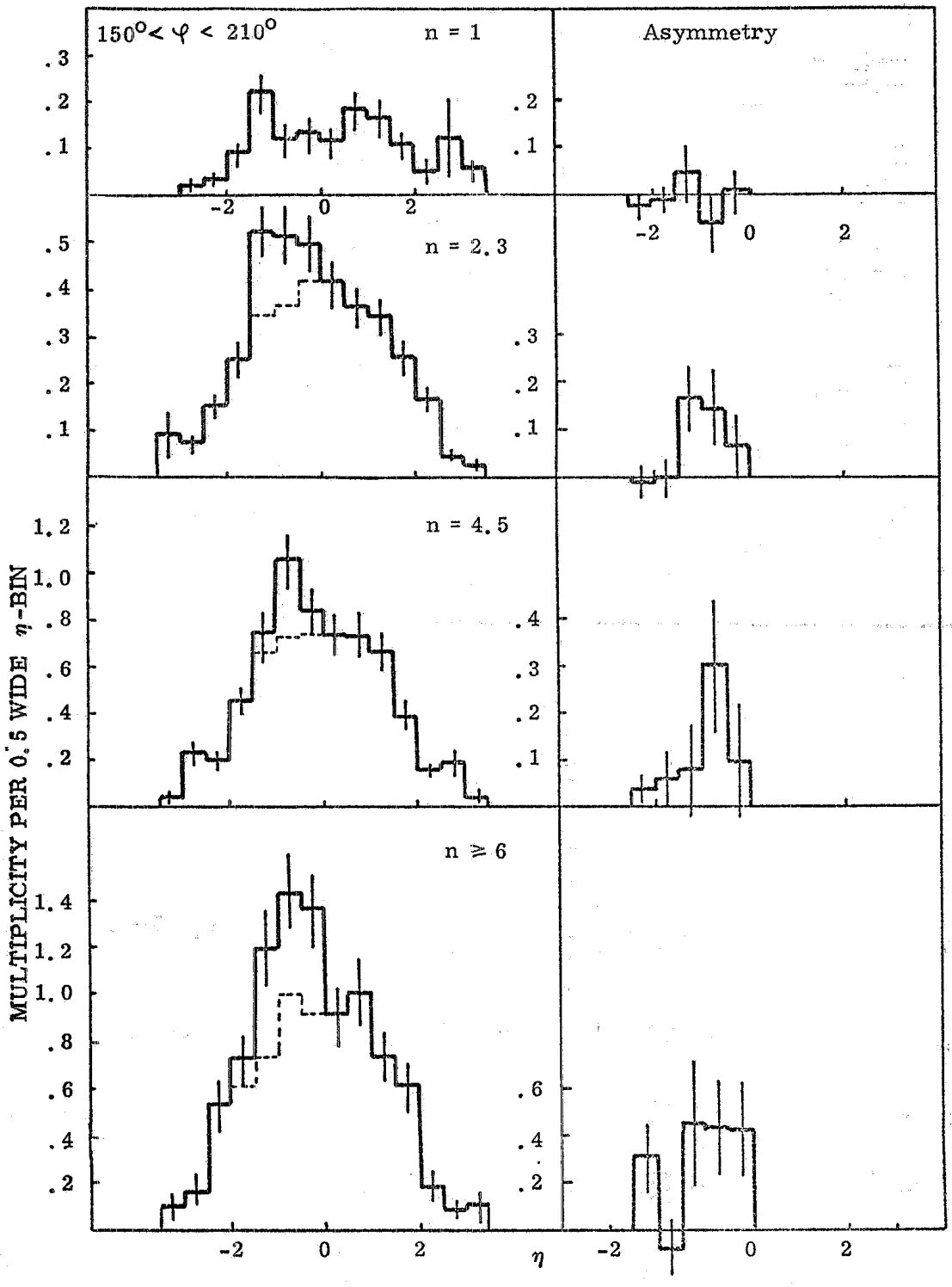

FIG. 29 - On the left side charged multiplicity distribution as a function of η for $150^{\circ} < \varphi < 210^{\circ}$ with respect to the triggering π^{o} (at $\phi = 0$, $\theta = 55^{\circ}$ viz. $\eta \sim 0.7$, and with $P_{\perp} \sim 3$ GeV/c); on the right side, difference with respect to the distributions obtained with an inclusive beam-beam trigger. From top to bottom, data obtained with different charged multiplicity seen in the interval $150^{\circ} < \varphi < 210^{\circ}$ (data from ACHM, ref. 13). Broken curves show distributions simmetric around $\eta = 0$.

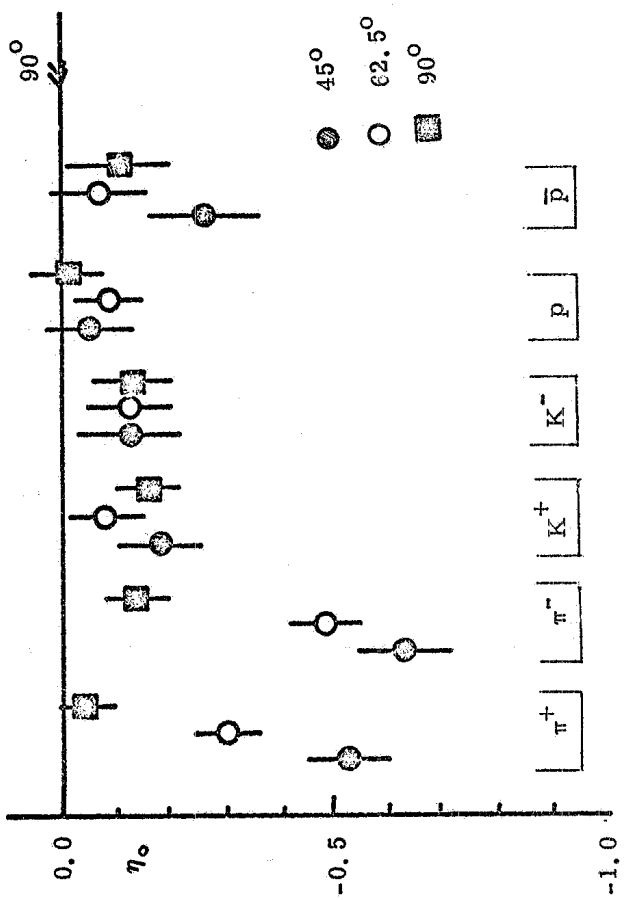

FIG. 31 - Location (η_o) of the peak of the η-distribution on the away hemisphere obtained with triggering π^+-, K^+-, p and $\bar{p}$ at θ_{cm} = 90°, 62.5° and 45° and for $P_\perp > 1$ GeV/c (data from DILR, ref. 13). η_o is expected to be zero when θ_{cm} = 90°. On bottom of figure, the symbol indicates the triggering particle for the three corresponding data points.

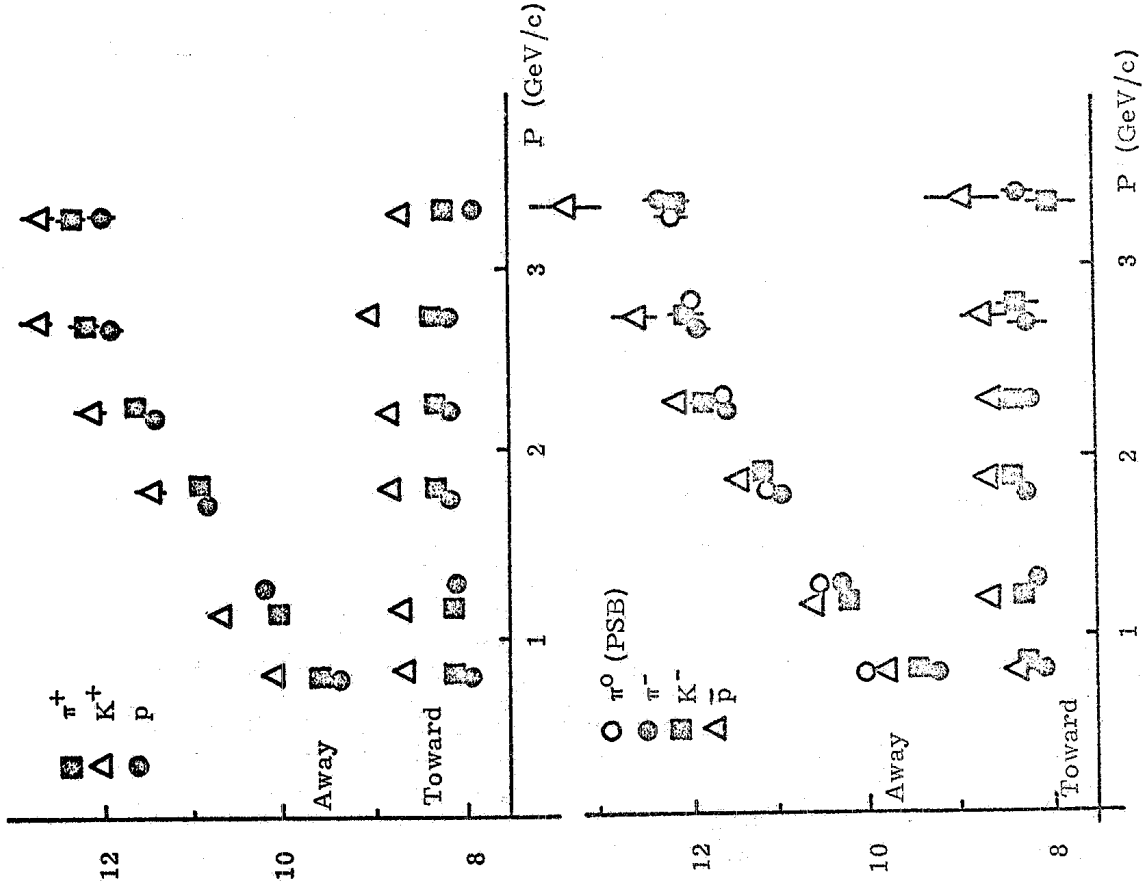

FIG. 30 - Total charged multiplicity as a function of $P_\perp$ of triggering $\pi^\pm$, $K^\pm$, p and $\bar{p}$. $\sqrt{s}$ = 44 GeV (data from DILR, ref. 13). PSB data obtained with a π^o trigger is also shown for comparison. Data for the two hemispheres, toward and away from the triggering particle, are plotted separately.

associated with $\pi^{\pm}$, $K^{\pm}$, p and $\bar{p}$ of large $P_\perp$ emitted at $\theta_{CM} = 90^o$, 62.5^o and 45^o. The experimental arrangement includes the wide angle magnetic spectrometer with threshold Cerenkov counters previously used by the British-Scandinavian Collaboration (Fig. 5) and a barrel counter hodoscope sorrounding the ISR intersection. Fig. 30 shows data of this group at $\sqrt{s} = 44$ GeV, which give the dependence of multiplicity on $P_\perp$ of the triggering particle ($\pi^{\pm}$, $K^{\pm}$, p and $\bar{p}$) at 90^o. One can see that independent of the nature of the triggering particle, the multiplicity on the away side increases lineraly with $P_\perp$ while it remains constant on the toward side. This result is in reasonable agreement with the PSB data (see Figure). However the DILR data taken at angles other than 90^o show that the centers η_o of the peak in the η distribution observed in the away side depend on the nature of the triggering particle. Fig. 31 illustrates such effect from the data taken at $\sqrt{s} = 44$ GeV, $P_\perp > 1$ GeV and at $\theta_{CM} = 90^o$, 62.5^o and 45^o ($\eta = 0$, 0.5 and 0.9). For $\pi^{\pm}$ as triggers, η_o moves to values roughly opposite to the corresponding η of the $\pi^{\pm}$. However, these peaks are centred at $\eta \approx 0$ in all cases when $K^{\pm}$, p and $\bar{p}$ are used as triggers, independent of their angle. These data, although preliminary, look quite interesting and seem to exhibit features of high $P_\perp$ reactions which are significantly different from what was known before.

It is obvious that the properties or even the existence of the large $P_\perp$ jet opposite to the large $P_\perp$ triggering particle could be better clarified if one measures not only the angles but also the momenta of all particles associated with the jet. To obtain this information, one would need a large acceptance multibody spectrometer similar to the split field magnet detector at ISR. Extensive data from this detector are not yet available at this time. However, some results along these lines were obtained from an experiment in which one measured, over a limited solid angle around 90^o, the momenta of charged particles accompanying or opposite to a large $P_\perp$ π^o. The experiment was performed by the CERN-Columbia-Rockefeller-Saclay (CCRS) Collaboration[1, b]. Fig.32

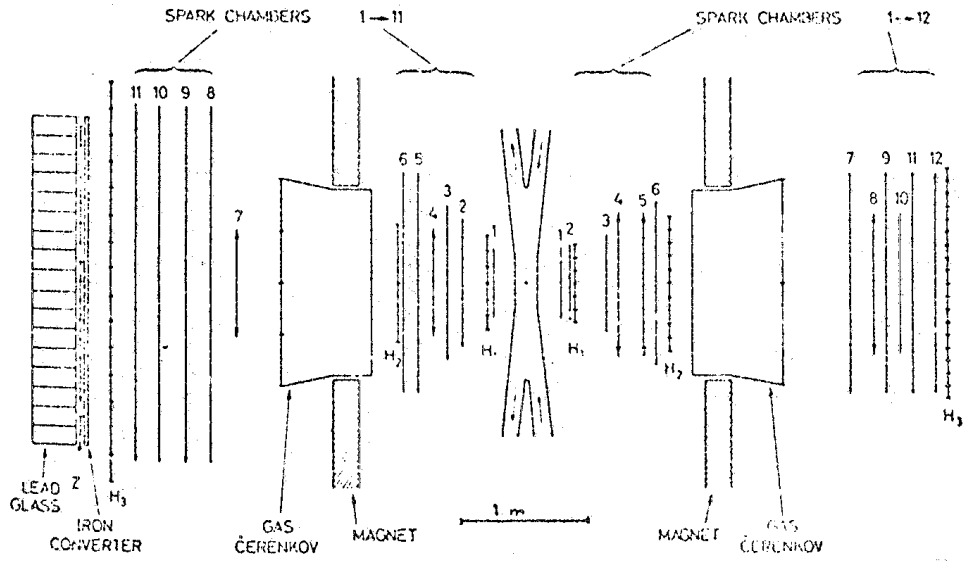

FIG. 32 - The experimental apparatus of CCRS group[1, b].

shows the CCRS experimental apparatus, which consisted of two magnetic spectrometers. While both arms can detect the charged particles and measure their momenta, photons from π^o decay are identified by the total absorption lead glass Cerenkov counters located at the end of one arm. Fig. 33 shows the charged particle $P_\perp$ spectra when the π^o and the charged particle are on the same side, while Fig. 34 shows the result on the opposite side. In both cases one can see, when one compares the distributions with the inclusive ones (also shown in the two figures), that the request of a large $P_\perp$ ($P_\perp > 3$ GeV/c) π^o being detected strongly biases the charged hadron spectrum and increases the probability of finding a large $P_\perp$ charged particle. At a first glance, it does not seem easy to reconcile these data, in particular the data of the same side correlation, with a naive two-jet picture.

A similar situation holds if one studies the probability of finding a second energetic π^o accompanying a first one at large angles. Data on this process have been collected by the CCR group[14] and are plotted in Fig. 35. The figure aims to show the momentum correlations between the two large

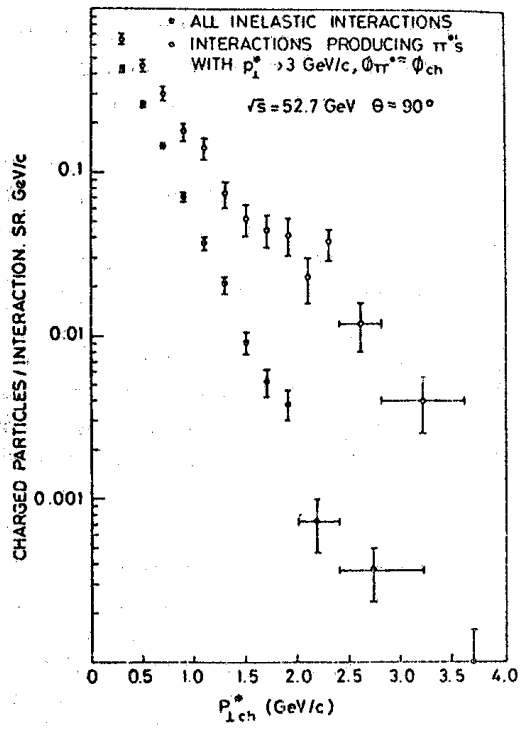

FIG. 33 - Momentum distribution of charged hadrons at 90° and opposite side as the π^0 (open circles) compaired to the unbiased inclusive distribution (full points) (Data from CCRS, ref. 1b).

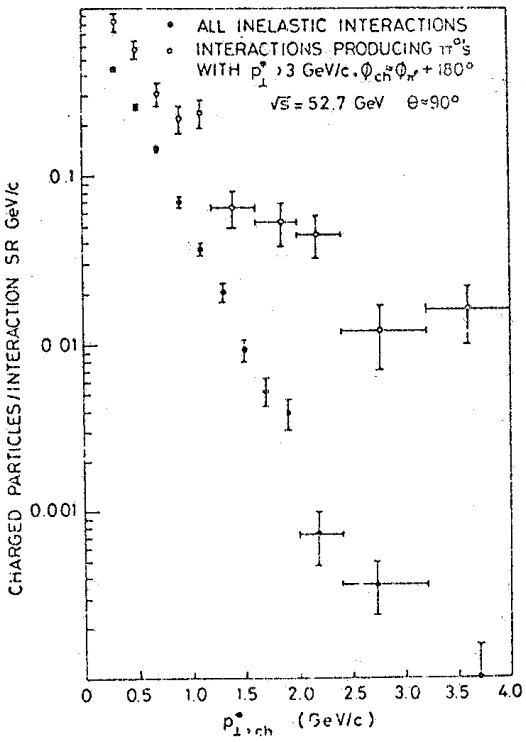

FIG. 34 - Momentum distribution of charged hadrons at 90° and same side as the π^0 (open circles) compaired to the unbiased inclusive distribution (full points) (Data from CCRS, ref. 1b).

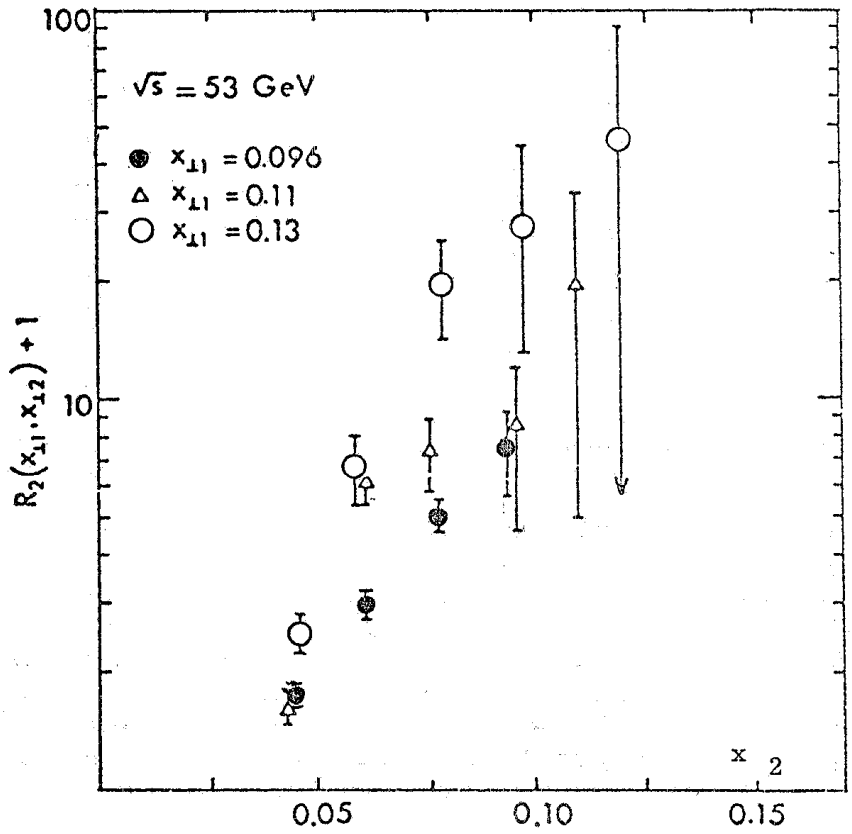

FIG. 35 - The correlation function $(R_2 + 1)$ for two π^0 of the same side (data from CCR, ref. 14).

$P_\perp$ π^o on the same side. The correlation function $R_2(x_1, x_2)$ is defined as

$$R_2(x_1, x_2) + 1 = \frac{\sigma_{INEL} \dfrac{d^6\sigma}{dp_{\perp 1}^3 dp_{\perp 2}^3}}{\dfrac{d^3\sigma}{dp_{\perp 1}^3} \dfrac{d^3\sigma}{dp_{\perp 2}^3}}$$

Again, the correlation function is largest for both x_1 and x_2 being largest.

The final comment on correlations in large $P_\perp$ events cannot, at the present moment, take the form of a firm conclusion. It is clear that, although kinematic plays an important role, a number of important effects exist which are not of kinematical origin. Very roughly these effects can be summarized in a two-jet picture. However we have seen a number of details which complicate this picture and which need further experimental studies and better understanding. A natural progress in this field is to be expected from experiments in which momenta of secondaries are measured over a very large solid angle. However this is a difficult task and results may not be available soon.

3.- INCLUSIVE DIRECT LEPTON PRODUCTION AT LARGE $P_\perp$.-

An extensive search for direct production of leptons, of high transverse momentum, at the highest energy accelerators was originally motivated as a way to discover the possible existence of the intermediate vector boson or of heavy leptons. Although no discovery of such a fundamental importance has yet been made, this search has resulted in the past two years in a rather strong excitement. The large cross section of the direct leptons which has been observed ($\approx 10^{-4}$ of the pion cross section) cannot easily be explained by either the decay of short-lived known resonances, and is sensibly larger than the expected rate from collisions between point-like constituents of hadrons[15]. More recently, it has been realized that also the recently discovered J, ψ resonances are not produced copiously enough to explain the observed rate of direct leptons.

Among the experiments that have reported results on this field[16] only three will be covered for simplicity:

1) $e^\pm$: CERN-Columbia-Rockefeller-Saclay Collaboration (CCRS) at the ISR, with $\sqrt{s} = 52.7$ GeV in p-p collisions.
2) $e^\pm$ and $\mu^\pm$: Columbia-FNAL Collaboration at Fermi Lab., with 300 GeV incident protons on a Be target.
3) $\mu^\pm$: Chicago-Princeton Collaboration at Fermi Lab., with 300 GeV incident protons on heavy targets.

At the ISR the CCRS Collaboration has studied single electrons of large $P_\perp$ from p-p collisions at 90° and $\sqrt{s} = 53$ GeV[17]. Fig. 36 shows the experimental set-up. The momentum is measured by a bending magnet and spark chambers and the identification of the electrons is done by the threshold Cerenkov counter inside the magnet. The lead glass hodoscopes at the back of the spectrometer give further electron identification and measurement of its energy. The requirement of the pulse height from a single minimum ionizing particle in the first counter hodoscope H_1' supresses events from Dalitz decay or from photon conversions which give very narrow e^-e^+ pairs. The rate of accepted events is found to depend very little on the thickness of additional converter placed in front of the telescope in order to increase artificially the background from electron pairs (Fig. 37, curve a)). On the other hand, the rate of e^-e^+ pairs (Dalitz π^o-decay+conversion) can also be monitored in the same way and shows, as expected, a steep dependence on the converter thickness and a residual at t = 0 which is consistent with the expected rate from Dalitz pairs (Fig. 37, curve b).

The average cross-section of e^- and e^+ direct production is plotted in Fig. 38 as a function of the energy of the lepton. The data for positive and negative electrons have been averaged because the cross section for e^-, within statistical error, is found to be the same as for e^+. The inclusive π^o spectrum from the CCR group is also plotted for comparison. To a first approximation, the electron spectrum differs from the π^o spectrum by just a scaling factor of 1.3×10^{-4}.

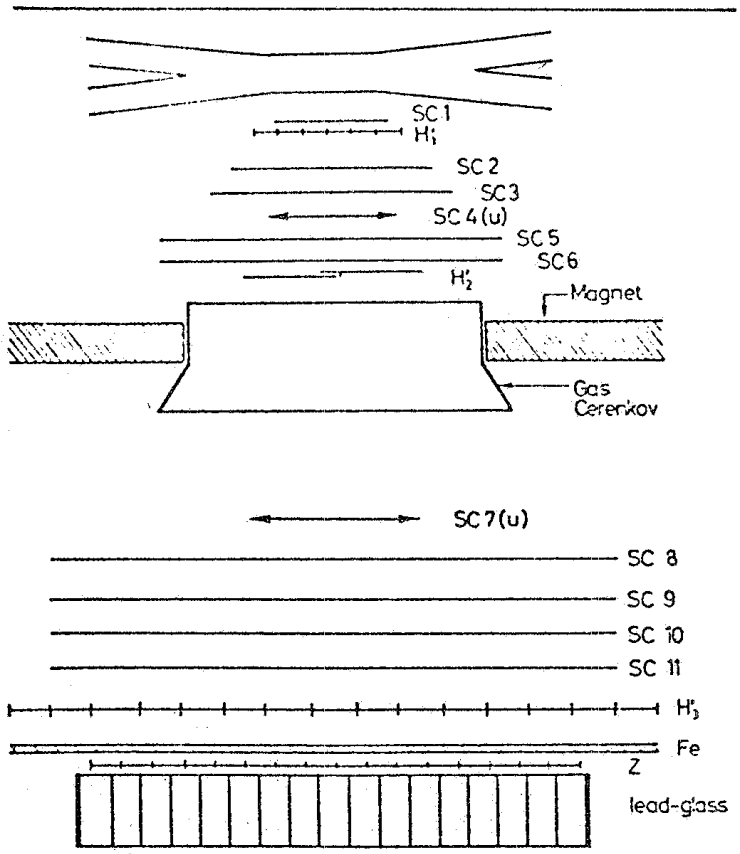

FIG. 36 - Experimental set up of the CCRS group for detecting electrons of high $P_\perp$ at 90^o (17).

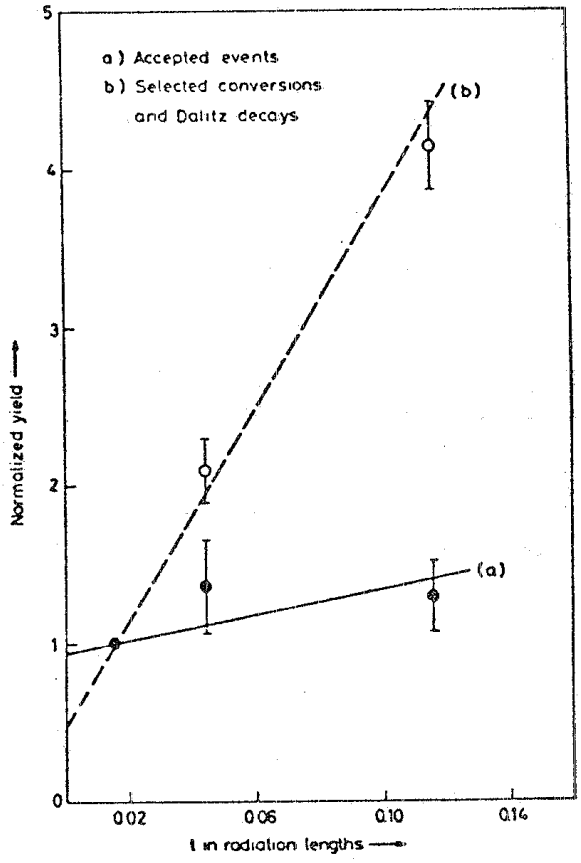

FIG. 37 - Integrated rates of CCRS experiment(17) as a function of added converter thichness in front of the telescope. The full points (●) are the data after applying the experimental cuts (direct production of single electrons) and the open circles (○) are the data requiring two or more particles in the first hodoscope H'_1.

The Columbia-FNAL Collaboration has measured both high $P_\perp$ electrons and muons of direct production at the Fermi Lab. with a 300 GeV incident proton beam on a Be target(18). Fig. 39 shows the experimental apparatus for the electron detection. The data were taken at production angles of 50 mr ($\theta_{CM} \simeq 65^o$) and 83 mr ($\theta_{CM} \simeq 93^o$). An electron produced at the Be target passes through a steel collimator, then is deflected vertically by a bending magnet. The system of magnet and scintillation hodoscopes determines the momentum of the particle. At the and of the spectrometer, there are a Pb-glass calorimeter and a steel-scintillator hadron detector for shower detection and hadron rejection. The lead-glass calorimeter is split into sections in order to check the early development of the electromagnetic shower which is typical of electrons. Fig. 40 shows a plot of event distribution as a function of E/P, where E = energy deposited in the lead glass and P = measured momentum of the charged particle. Curve a) corresponds to all triggers. Normally for a electron E/P = 1 and for a pion E/P < 1. However hadrons sometimes leave a large fraction of their energy in the lead glass and appear as background under the electron peak at E/P > 0.9. If one applies cuts on the longitudinal shower development in the lead glass hodoscopes, one obtains the curve b). Curve c) is obtained from a pure hadron beam. The result of subtraction of curve c) from curve b) gives the electron signal. In Fig. 41, the yield of electron is plotted as a function of the thickness of additional converter in front of the spectrometer. The rate of direct electrons was obtained by extrapolating to zero converter thickness and subtracting the calculated contribution from Dalitz decay (which corresponds to 0.8% of a radiation length). The average invariant cross section for direct e^- and e^+ is given in Fig. 42 as a function of $P_\perp$, for both $\theta = 50$ mr and $\theta = 83$ mr. In order to obtain

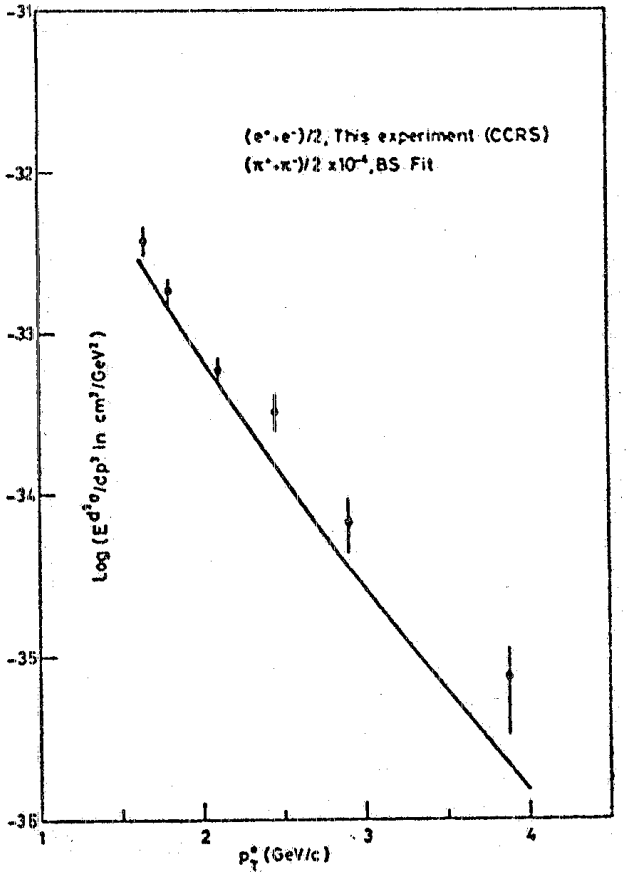

FIG. 38 - The average cross section for e^- and e^+ direct production as a function of the energy of the lepton detected at 90° and at $\sqrt{s} = 53$ GeV. The π^0 spectrum from CCR group is also plotted for comparison[17].

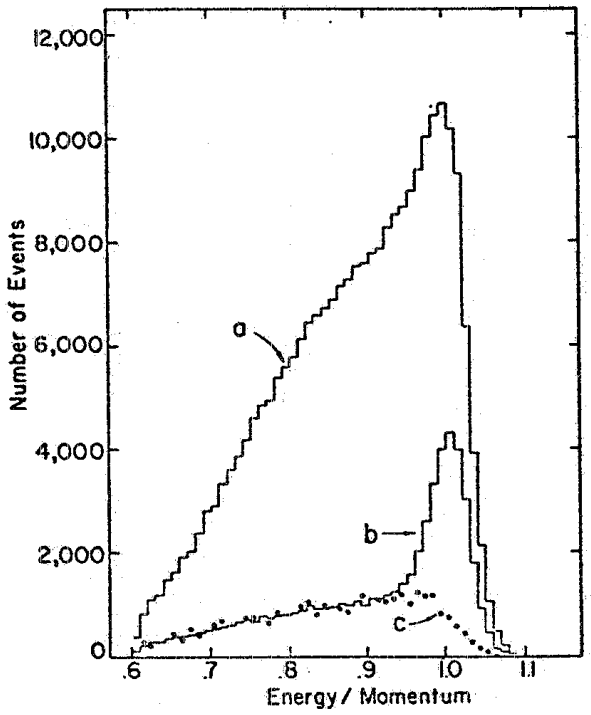

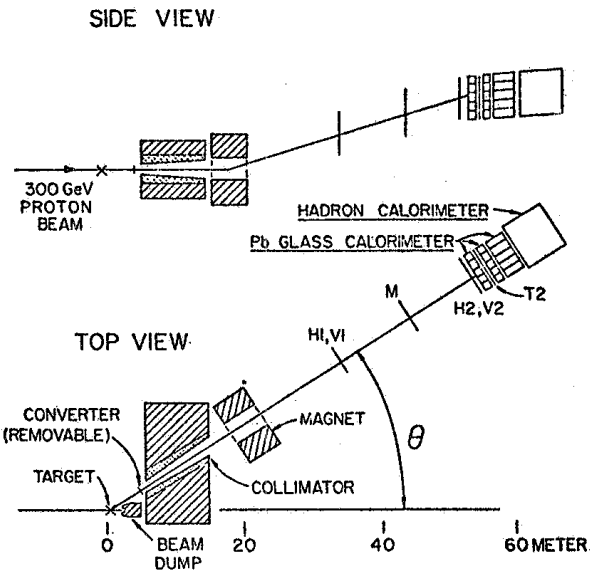

FIG. 39 - Experimental apparatus of the Columbia-FNAL experiment for electron detection at FNAL[18].

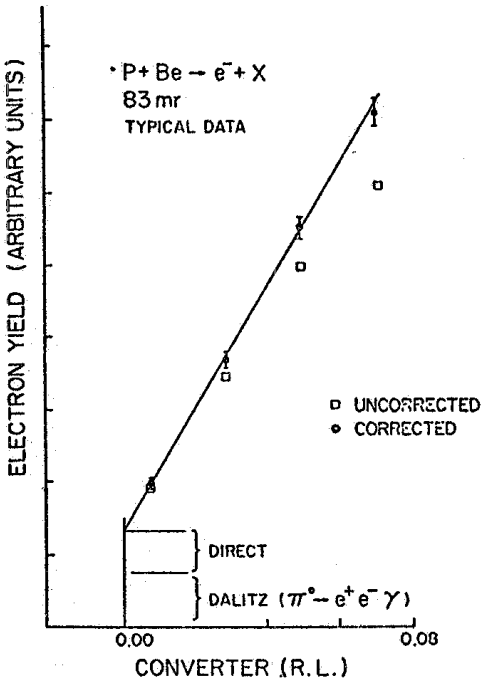

FIG. 41 - Electron yield as a function of converter thickness[18]. Corrections were made for electron energy loss due to bremsstrahlung.

FIG. 40 - Event distribution as a function of E/P[18]. Curve a): all triggers. Curve b): with cuts to signal electromagnetic showers in the lead-glass. Curve c): distribution from pure hadron beam.

the cross-section on nucleon, the Berillium data have been divided by 9, the Berillium mass number. Although this procedure leaves a large uncertainty (factor of 2) in the absolute cross-section, the electron/π^0 ratio is measured much better, since the π^0 flux is also monitored directly in the same experiment (from the slope found in Fig. 41). At both angles one finds a cross-section which is about 10^{-4} of the cross section of π^0 production.

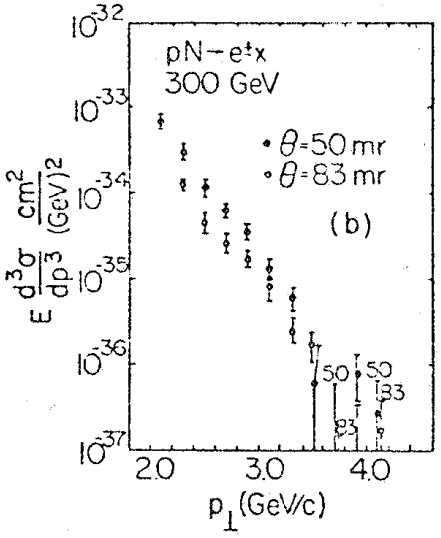

FIG. 42 - The average invariant cross section for e^+ and e^- at p_{LAB} 300 GeV, both $\theta = 50$ mr and $\theta = 83$ mr.

In the same Fermi Lab. experiment[18] muons were also monitored by inserting a movable heviment filter near the target to vary the decay path of pions and kaons. After correcting for different spectrometer acceptance at different converter thickness, the extrapolation to zero decay path gives the direct production of single muons as shown in Fig. 43. The invariant cross sections as a function of $P_\perp$ for μ^- and μ^+ are shown in Fig. 44 for $\theta_{CM} \approx 90^\circ$. Again the yields for μ^- and μ^+ are the same and they are consistent with the $e^\pm$ yields.

Next, we shall describe the experiment done by the Chicago-Princeton group at the Fermi Lab.[19]. They have detected direct muons produced by a 300 GeV incident proton beam on Cu and W targets, at angles corresponding to $\approx 90^\circ$ in the nucleon-nucleon center of mass system. The experimental set up is as shown in Fig. 11 except for two absorbers which were inserted into the spectrometer close to the target in order to separate the direct muons from the muons coming from π and K decays. By inserting or removing different combinations of these absorbers, they obtained the muon yield as a function of decay path. Again, the extrapolation to zero decay path gives the direct yield. Fig. 45 gives the μ/π ratio as a function of distance from the target. The dashed line shows the extrapolation to zero decay length and the solid line is the calculated slope. The invariant cross section of the direct muons as a function of $P_\perp$ from 1.5 to 5.4 GeV/c is given in Fig. 46. The cross section on nucleon is derived from the data after dividing for the effective mass number of the target nucleus, and is subject to a large systematic error. However, since in this experiment one can measure the π cross section at the same time, the μ/π ratio is much better determined. The corresponding π^+ inclusive cross section x 10^{-4} is given by the solid curve in this figure. The dashed line is the calculated cross section from a parton-antiparton annihilation model. One concludes again that the μ/π ratio is about 10^{-4}, independent of $P_\perp$. One sees also that the direct muon production is about one to two orders of magnitude larger than the prediction from parton models.

To conclude, one learns from the results on the direct production of leptons of high $P_\perp$:

1) The ratio of e/π or μ/π is constant and independent of $P_\perp$ (for $1.5 \lesssim P_\perp \lesssim 5.5$ GeV/c) and of $\sqrt{s}$ (for $20 \lesssim \sqrt{s} \lesssim 62$ GeV). This ratio is about 10^{-4}.

2) The cross section falls smoothly over 6 decades from $P_\perp \sim 1.5$ GeV/c to $P_\perp \sim 5.5$ GeV/c with no signature of bumps. It is therefore very unlikely that these leptons are produced in two-body decays of mesons (for instance the new particles) in the mass range $3 \lesssim M \lesssim 11$ GeV.

3) The source of these direct leptons still needs to be explained. The cross section is one or two orders of magnitude higher than the prediction of parton models. Leptonic decays of vector mesons, which are the most natural candidates for direct production of single leptons, cannot be totally ruled out as the main source of the observed rate, but calculations show that in this case they would have to be produced surprisingly aboundantly.

Of course, leptonic three-body decays of new heavy particles, like charmed particles, could possibly be the origin of the phenomenon. If this was the case, pair production of charmed particles would give rise to large rates of coincident electron-electron, muon-muon, and electron-muon pairs. Experiments which are in progress on direct production of lepton pairs will shed light on this possibility. Additional essential information is likely to be provided by correlation experiments between single leptons or lepton pairs and the associated hadronic production.

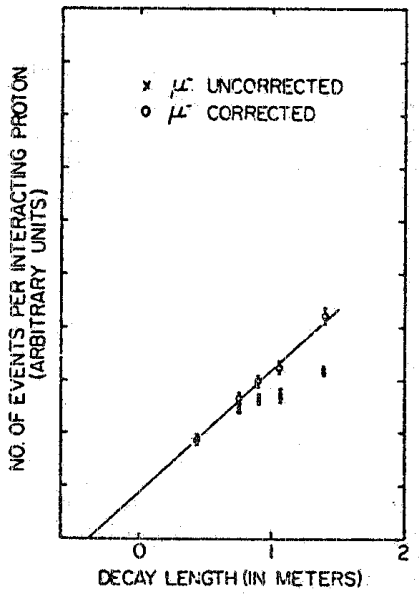

FIG. 43 - μ^- yield as a function of decay length from target to absorber(18). Corrections have been applied to account for the change in acceptance produced by the different level of arm of multiple scattering in different absorbers.

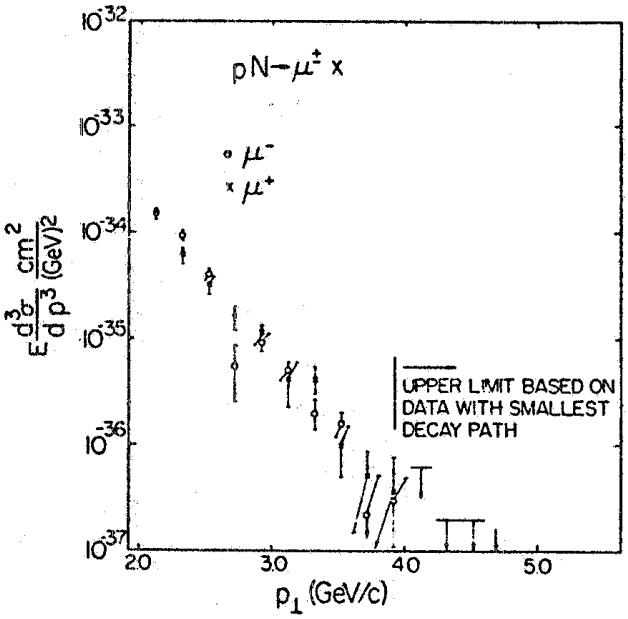

FIG. 44 - The invariant cross sections for directly produced μ^- and μ^+ at $\theta_{CM} \sim 90^o$ (18).

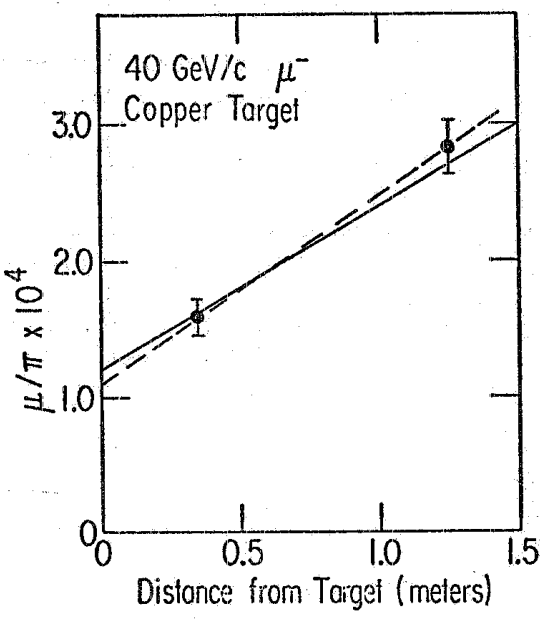

FIG. 45 - μ/π ratio as a function of effective distance of absorber from the target(19). The dashed line is the linear extrapolation to zero decay length and the solid line is the calculated slope.

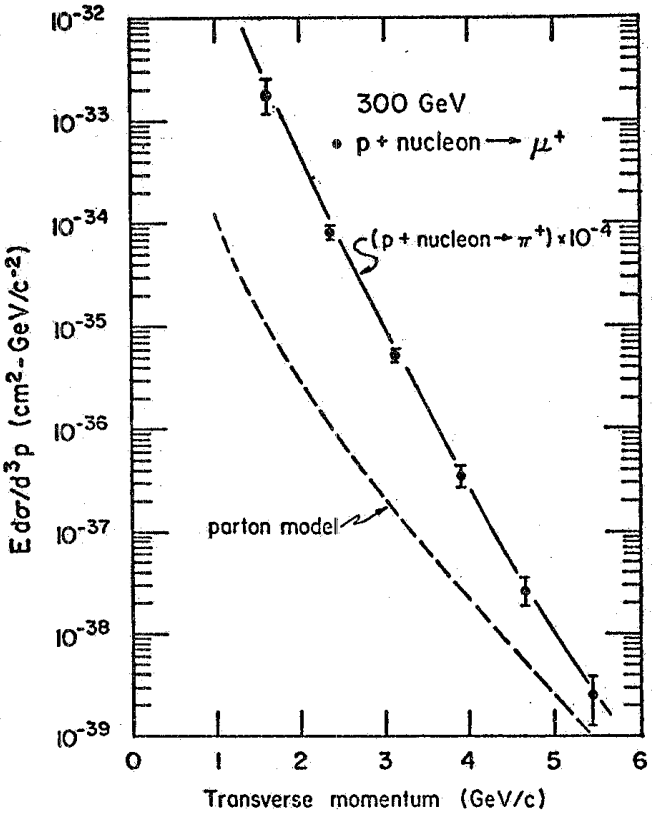

FIG. 46 - The invariant cross section for direct μ^+ production as a function of $P_\perp$. The solid line is π^+ production X 10^{-4} and the dashed line is the prediction from a parton model.

REFERENCES. -

(1) - See the Proceeding of the seventeenth Intern. Conf. on High Energy Physics, London, England, 1-10 July 1974. a) Large Transverse Momentum Reactions by P. V. Landshoff (V-57 to V-81). b) Correlations in High Transverse Momentum Final States by L. Di Lella (V-13 to V-20). c) Theoretical Models for Large Transverse Momentum Phenomena by S. D. Ellis (V-23 to V-40). Also see d) Large Transverse Momentum Phenomena, An Experimental and Theoretical Review by S. D. Ellis and R. Thun, CERN-TH-1874.

(2) - See Table 2.1 of P. V. Landshoff's rapporteur talk of reference (1).

(3) - F. W. Büsser et al., Phys. Letters 46B, 471 (1973).

(4) - S. M. Berman and M. Jacob, Phys. Rev. Letters 25, 1683 (1970); S. M. Berman, J. D. Bjorken and J. B. Korgut, Phys. Rev. D4, 3388 (1971).

(5) - F. W. Büsser et al., Phys. Letters 55B, 232 (1975).

(6) - B. Alper et al., Nuclear Phys. B87, 19 (1975).

(7) - J. W. Cronin et al., Phys. Rev. Letters 31, 1426 (1973).

(8) - The data were obtained with tungsten as target. An effective number of nucleons is defined as $A_{eff} = \sigma_{abs}/\sigma_p = 1635/40 = 40.9$ where σ_{abs} is the absorption cross section in W(1635 mb) and σ_p is the p-p total cross section (40 mb). A large systematic uncertainty is attached to this method of deriving nucleon-nucleon cross-sections from nucleon-nucleus data.

(9) - G. Finocchiaro et al., Phys. Letters 50B, 396 (1974).

(10) - Charged particle multiplicities associated with large transverse momentum photons at the ISR, by G. Finocchiaro et al., submitted to the XVII Intern. Conf. on High Energy Physics, London 1974; See also refs. (1a) and (1b).

(11) - S-dependence of charged particle multiplicities associated with large transverse momentum photons at the ISR, R. Kephat et al., submitted to the XVII Intern. Conf. on High Energy Physics, London, 1974; See also refs. (1a) and 1b).

(12) - Observation of Proton-Proton Interactions with π^o of large transverse momentum at the ISR by B. Betev et al., submitted to the XVII Intern. Conf. on High Energy Physics, London, 1974.

(13) - These results can be found in the report prepared by M. Jacob (TH Division, CERN) on The structure of large transverse momentum events, (ISR Discussion Meeting between experimentalists and theorists, meeting number 13).

(14) - F. W. Büsser et al., Phys. Letters 51B, 311 (1974).

(15) - a) S. D. Drell and T. M. Yan, Phys. Rev. Letters 25, 1523 (1970); b) J. D. Bjorken, Proceedings of the second Intern. Conf. on High Energy Particles, Aix-an-Provence (1973); Journal de Physique, 34, 1426 (1973).

(16) - See Table 3.1 of reference 1, a). Also see the section on the observation of leptons of large transverse momentum, of the Proceeding of the XVII Intern. Conf. on High Energy Physics, London 1974 (from V-41 to V-55).

(17) - F W. Büsser et al., Phys. Letters 53B, 212 (1972); Also S. L. Segler, in Proceedings of the Seventeenth Intern. Conf. on High Energy Physics, London, 1974 (V-41 to V-43).

(18) - J. A. Appel et al., Phys. Rev. Letters 33, 722 (1974); Also T. Yamanouchi, in Proceedings of the Seventeenth Intern. Conf. on High Energy Physics, London, England, 1-10 July 1974 (V-43 to V-46).

(19) - J. P. Boymond et al., Phys. Rev. Letters 33, 112 (1974); Also P. A. Pirone, in Proceedings of the Seventeenth Intern. Conf. on High Energy Physics, London, England, 1-10 July 1974 (V-47 to V-49).